Development 140, 93-106 (2013) doi:10.1242/dev.087825

Sim1a and Arnt2 contribute to hypothalamo-spinal axon guidance by regulating Robo2 activity via a Robo3-dependent mechanism

Jörn Schweitzer[1,*,§], Heiko Löhr[1,*,‡], Joshua L. Bonkowsky[2], Katrin Hübscher[1] and Wolfgang Driever[1,3,§]

SUMMARY

Precise spatiotemporal control of axon guidance factor expression is a prerequisite for formation of functional neuronal connections. Although Netrin/Dcc- and Robo/Slit-mediated attractive and repulsive guidance of commissural axons have been extensively studied, little is known about mechanisms controlling mediolateral positioning of longitudinal axons in vertebrates. Here, we use a genetic approach in zebrafish embryos to study pathfinding mechanisms of dopaminergic and neuroendocrine longitudinal axons projecting from the hypothalamus into hindbrain and spinal cord. The transcription factors Sim1a and Arnt2 contribute to differentiation of a defined population of dopaminergic and neuroendocrine neurons. We show that both factors also control aspects of axon guidance: Sim1a or Arnt2 depletion results in displacement of hypothalamo-spinal longitudinal axons towards the midline. This phenotype is suppressed in *robo3* guidance receptor mutant embryos. In the absence of Sim1a and Arnt2, expression of the *robo3* splice isoform *robo3a.1* is increased in the hypothalamus, indicating negative control of *robo3a.1* transcription by these factors. We further provide evidence that increased Robo3a.1 levels interfere with Robo2-mediated repulsive axon guidance. Finally, we show that the N-terminal domain unique to Robo3a.1 mediates the block of Robo2 repulsive activity. Therefore, Sim1a and Arnt2 contribute to control of lateral positioning of longitudinal hypothalamic-spinal axons by negative regulation of *robo3a.1* expression, which in turn attenuates the repulsive activity of Robo2.

KEY WORDS: Robo/Slit signalling, Robo receptor isoforms, Dcc/Netrin signalling, Dopaminergic neurons, Neuroendocrine systems, Hypocretinergic neurons, Hypothalamo-spinal projections, Orthopedia, Zebrafish

INTRODUCTION

Understanding how transcription factors genetically encode the specification of connectivity in the nervous system is a challenge in neurobiology. Knowledge of molecular mechanisms that link transcription factor function to regulation of axon guidance in vertebrates is limited to a few well-studied systems, including spinal motoneuron projections and retinotectal trajectories (for a review, see Butler and Tear, 2007; Polleux et al., 2007). However, for most central nervous system projection pathways, it is unknown how connectivity is transcriptionally determined.

Hypothalamic projections into the spinal cord (HTS) are an attractive model for understanding how CNS nuclei establish long-range projections. A well-characterised transcriptional network specifies hypothalamic cell lineages. The homeodomain transcription factor Orthopedia (Otp) is co-expressed with the two PAS domain factors Sim1 and Arnt2, the latter two forming functional heterodimers. Otp/Sim1/Arnt2-dependent cell lineages in mammals (Acampora et al., 1999; Michaud et al., 2000; Michaud et al., 1998; Wang and Lufkin, 2000) and zebrafish (Blechman et al., 2007; Del Giacco et al., 2006; Eaton and Glasgow, 2006; Eaton and Glasgow, 2007; Löhr et al., 2009; Ryu et al., 2007) include neuroendocrine cells characterised by expression of the peptide hormones corticotropin-releasing hormone, thyrotropin-releasing hormone, arginine vasopressin, oxytocin and somatostatin. In addition to neuroendocrine lineages, Otp/Sim1/Arnt2 have been shown to control development of hypothalamic A11-type dopaminergic (DA) neurons in zebrafish and, for Otp, mammals (Borodovsky et al., 2009; Löhr et al., 2009; Ryu et al., 2007). Despite the diverse neurotransmitter/neuropeptide phenotypes, Otp/Sim1/Arnt2-specified cell types share similar descending ipsilateral projections. Neuroendocrine cell lineages have been shown to innervate spinal target fields in mammals (Hancock, 1976; Swanson, 1977) and zebrafish (M. Hammerschmidt, personal communication). Furthermore, A11-type DA neurons project directly to the spinal cord in mammals (Björklund and Skagerberg, 1979) and zebrafish (Tay et al., 2011). The similarity in projection patterns of diverse Otp/Sim1/Arnt2-specified hypothalamic neurons prompted us to investigate whether this transcription factor network might also regulate axon guidance.

Ipsilateral longitudinal axon guidance is regulated in part by the Robo/Slit and Netrin/Dcc receptor/ligand pairs (Farmer et al., 2008; Kastenhuber et al., 2009). Slit and Netrin guidance cues are expressed by ventral midline cells and bind to receptors of the Robo and Dcc families, respectively (Brose et al., 1999; Keino-Masu et al., 1996). In mouse, loss of the two Robo receptors Robo1 or Robo2, as well as loss of Slit1 and Slit2 ligands, disrupts proper establishment of longitudinal pioneer tracts in the midbrain and hindbrain (Farmer et al., 2008), and Robo/Slit signalling also affects ascending nigrostriatal tracts of mesencephalic dopaminergic neurons (Dugan et al., 2011). Similarly, longitudinal axons of A11-related DA

[1]Developmental Biology, Institute Biology 1, Faculty of Biology, University of Freiburg, Hauptstrasse 1, D-79104 Freiburg, Germany. [2]Department of Pediatric Neurology and Pediatrics, University of Utah, School of Medicine, Salt Lake City, UT 84132, USA. [3]BIOSS Centre for Biological Signalling Studies and FRIAS Freiburg Institute for Advanced Studies, University of Freiburg, Albertstrasse 19, D-79104 Freiburg, Germany.

*These authors contributed equally to this work
‡Present address: Institute for Developmental Biology, University of Cologne, Zuelpicher Strasse 47b, 50674 Cologne, Germany
§Authors for correspondence (joern.schweitzer@biologie.uni-freiburg.de; driever@biologie.uni-freiburg.de)

Accepted 3 October 2012

neurons in zebrafish integrate midline repulsion via Robo2/Slit and midline attraction via Dcc/Netrin1 to specify lateral positioning (Kastenhuber et al., 2009). A role for Robo3 during ipsilateral longitudinal axon guidance has not been reported. Robo3, with at least four splice variants (Ypsilanti et al., 2010), displays the greatest structural heterogeneity within the Robo receptor family, and controls pre- and post-crossing behaviour of commissural axons (Chen et al., 2008; Sabatier et al., 2004).

Here, we provide evidence that Arnt2 and Sim1a are required to determine the lateral position of neuroendocrine and DA longitudinal axons en route to the spinal cord. Loss of Arnt2 or Sim1a function leads to displacement of HTS axons towards the midline. By performing expression analyses together with gain- and loss-of-function studies, we show that the abnormal projection pattern observed is caused by misexpression of the specific Robo3 isoform *robo3a.1*. We further show that Robo3a.1 is sufficient to block Robo2-mediated midline repulsion of HTS longitudinal axons. Our data suggest that Sim1a and Arnt2 negatively regulate *robo3a.1*, which in turn attenuates repulsive activity of Robo2, and thereby controls the lateral positioning of HTS longitudinal axons.

MATERIALS AND METHODS

Fish maintenance and strains

Zebrafish were maintained at 28.5°C (Westerfield, 1995). To inhibit pigmentation, embryos were incubated in 0.2 mM phenylthiourea. For a complete list of used zebrafish lines, see supplementary material Table S1. Compound mutants were identified by PCR. Genotyping of *arnt2*^{hi2639c}, *ast*^{ti272z}, *ast*^{te284} and *twt*^{tw204} alleles was previously described (Chalasani et al., 2007; Fricke et al., 2001; Golling et al., 2002; Kastenhuber et al., 2009).

Immunohistochemistry and *in situ* hybridization

Whole-mount immunohistochemistry (Holzschuh et al., 2003), *in situ* hybridization and fluorescent *in situ* hybridization were performed as described previously (Filippi et al., 2007). To enhance signal intensity in fluorescent *in situ* hybridization, 5% dextrane sulphate was added in the hybridization buffer and 450 μg/ml iodophenol during peroxidase reaction. For confocal microscopy stained embryos were embedded in medium containing 1.2% low melting agarose in 80% glycerol. For details on antibodies and probes used, see supplementary material Table S2.

Plasmid construction and injections

For expression constructs, a multisite Gateway system was used (Kwan et al., 2007). For details on generation of constructs see supplementary material Table S3. For transient overexpression analyses and generation of stable lines, 25 pg plasmid and 50 pg Tol2 transposase RNA (*pCS2FA-transposase*) (Kwan et al., 2007) were co-injected into one-cell stage embryos.

Morpholino injections and photomorph experiments

Morpholino oligonucleotides (MOs) were obtained from Gene Tools (Philomath, OR). The *sim1a* (sim1a e2i2), *arnt2* (*arnt2* e2i2) and *dcc* (*dcc*-MO2) morpholinos have been described previously (Löhr et al., 2009; Suli et al., 2006). For controls, standard negative control morpholino from Gene Tools was used. Morpholinos were injected at one-cell stage: 0.25-1.0 ng (*sim1a* MO), 1-4.5 ng (*arnt2* MO) and 4.5 ng (*dcc* MO) per embryo.

Photomorph 2.0 caging strand (SuperNova Life Science) was designed to bind and block the *sim1a* morpholino. Prior to injection, caging strand and *sim1a* morpholino were mixed at a molar ratio of 7:1 and hybridised at 70°C for 30 minutes. Subsequently, the mixture was cooled down to 4°C and stored overnight prior to injection. Special care was taken to keep the caged MO solution and injected embryos in the dark until time of uncaging. Uncaging of the morpholino was performed by exposure to UV light (Peqlab, UV superbright light table, 312 nm, 100% intensity) for 30 minutes. Efficiency and function of the Photomorph caging strand was confirmed by PCR on cDNA derived from embryos injected with Photomorph caging strand and *sim1a* MO (with and without UV light treatment) using primers as described previously (Löhr et al., 2009).

Microscopy, quantification and statistical analyses

Confocal *z*-stacks were recorded using Zeiss LSM 510. LSM or NIH ImageJ software was used to create *z*-projections. Adobe Photoshop or Illustrator were used to assemble figures. Distances between axons were determined using Zeiss LSM510 Software. Midline crossing of MA axons was determined using a Leica MZ16F stereomicroscope. Quantification of fluorescence from in situ hybridization analyses: to determine the regions of interest for single neurons, we used the GFP channel and the region of interest manager embedded in ImageJ. Ten neurons in the anterior and six neurons in the posterior hypothalamus (see Fig. 4J) were randomly selected per embryo; on average, three slices per fish were used. To measure the average signal intensity within each selected neuron, as outlined by the regions of interest, we switched to the channel carrying the gene expression information maintaining the region of interest masks from the GFP channel. All samples were analysed at the LSM510 using identical acquisition parameters. Statistical analysis was performed using Student's *t*-test. Error bars represent s.d.

RESULTS

A novel role for Sim1 and Arnt2 in establishment of HTS axon tracts

Absence of Otp, Sim1 or Arnt2 results in loss of cell type-specific terminal differentiation markers of defined hypothalamic neuroendocrine cell groups and of A11-related DA neurons in zebrafish (Löhr et al., 2009; Ryu et al., 2007). Although not fully differentiated, these cells are maintained at least until 4 dpf, as judged by persistent expression of *otp* and *sim1* transcripts. To study the role of Sim1a and Arnt2 during longitudinal HTS tract formation, we used a transgenic zebrafish line visualizing *otpb*-expressing neurons in the hypothalamus and their longitudinal projections towards the spinal cord by GFP (supplementary material Fig. S1) (Fujimoto et al., 2011). To analyse a potential effect of Sim1a on HTS tract formation, we injected a *sim1a* morpholino into *otpb:gfp* transgenic embryos. *otpb:gfp*-positive longitudinal axons were significantly displaced towards the midline after depletion of *sim1a* when compared with controls (Fig. 1A-D,I; supplementary material Table S4). A similar medial displacement of *otpb:gfp* longitudinal HTS axons was observed upon injection of *arnt2* MO (Fig. 1E,F,I; supplementary material Table S4) and in *arnt2*^{hi2639c} mutant embryos (supplementary material Fig. S2A-E; Table S4). Moreover, co-injection of sub-threshold amounts of *sim1a* (0.25 ng) and *arnt2* (1.0 ng) morpholinos, which do not display a phenotype when injected individually, did result in a medial displacement of *otpb:gfp* HTS axons (Fig. 1G,H,I; supplementary material Table S4). To determine the specificity of the observed phenotype, we used a transgenic reporter line that labels hypocretinergic (Hcrt) neurons (*hcrt:tdtomato*). Hcrt neurons reside in the lateral hypothalamus and also project to spinal target regions (Faraco et al., 2006; van den Pol, 1999), but do not depend on Sim1a and Arnt2 transcription factors for differentiation (data not shown). Analysis of *otpb:gfp;hcrt:tdtomato* transgenic embryos revealed that HTS axons of Hcrt neurons and *otpb:gfp*-positive neurons run at similar mediolateral positions, yet longitudinal axons of Hcrt neurons did not display any change in lateral positioning upon *sim1a* knockdown (supplementary material Fig. S3A-G, Table S4). These results demonstrate that *sim1a* and *arnt2* are selectively and synergistically required for lateral positioning of *otpb:gfp*-positive HTS axons.

Temporally controlled knockdown links Sim1 function to axonal pathfinding of dopaminergic neurons

The medial displacement of *otpb:gfp* HTS axons upon depletion of *arnt2* and *sim1a* could be caused by transdifferentiation of DA (and

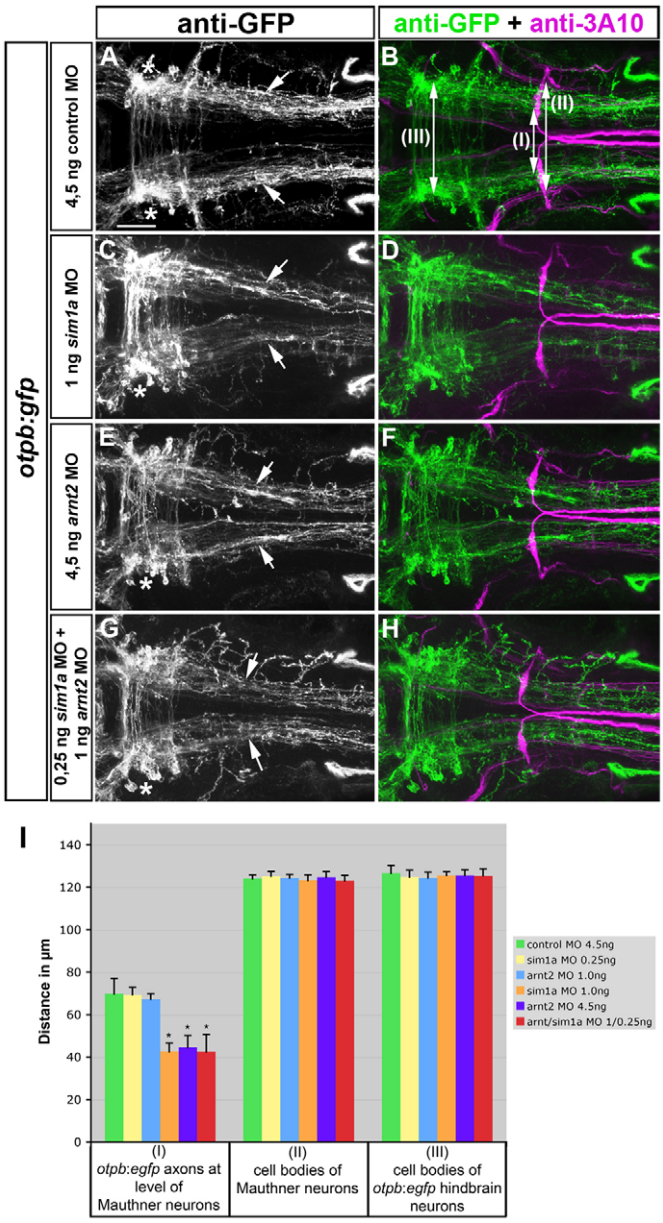

Fig. 1. Sim1a and Arnt2 act synergistically during longitudinal HTS axon guidance. Dorsal views of hindbrain confocal *z*-projections of *otpb:gfp* transgenic embryos at 72 hpf. Anterior is towards the left. (**A-H**) Mediolateral positioning of *otpb:gfp* axons (arrows) after indicated treatments. *otpb:gfp* hindbrain neurons (asterisks in A,C,E,G) do not contribute to longitudinal projections. (**I**) Quantification of the distance between *otpb:gfp* axons (I), of the distance between MA neurons (II) or between *otpb:gfp* hindbrain neurons (III). *P<0.0001 for *sim1a* MO 1.0 ng, *arnt2* MO 4.5 ng, *arnt2/sim1a* MO 1.0/4.5 ng versus control MO 4.5 ng. Scale bar: 50 µm.

neuroendocrine) cells into other cell lineages. To ascertain whether Sim1 is instructional for proper HTS pathfinding of DA neurons, we performed a temporally controlled loss-of-function experiment. We decided to knock down *sim1a* at a time point when DA terminal differentiation marker tyrosine hydroxylase (TH) expression has already been initiated, but HTS development is still ongoing. The *sim1a* morpholino was kept inactive by hybridization with a complementary caging strand (Tomasini et al., 2009) until uncaging and activation of the *sim1a* morpholino was achieved by photocleavage (supplementary material Fig. S4). Injection of *sim1a* morpholino resulted in complete loss of TH expression of A11-related DA cells and their HTS projections (Fig. 2C,D). Conversely, caged *sim1a* morpholino-injected embryos displayed the full complement of hypothalamic DA neurons and developed HTS tracts similar to controls (Fig. 2A,B,E,F). Next, we injected a caged *sim1a* morpholino and photo-activated the morpholino at 22 hpf. This time point was chosen, because the earliest A11-related DA neurons differentiate between 18 and 24 hpf. Following this treatment, we detected individual TH-positive DA neurons in 84% of the embryos analysed. These embryos displayed a significant medial displacement of TH-positive HTS axons (Fig. 2G,H,I; supplementary material Table S5). This reveals that Sim1a is essential for lateral positioning of DA HTS axons, and thus has multiple functions during distinct steps of DA cell differentiation and maturation.

Robo2 is required for lateral positioning of HTS axon tracts in Sim1a- and Arnt2-dependent and -independent cell lineages

Proper formation of DA HTS tracts requires Robo2 function (Kastenhuber et al., 2009). As DA neurons are a fraction of *otpb:gfp*-positive cells, we analysed whether the role of Robo2 applies to *otpb:gfp* longitudinal axons in general. Owing to similarities in longitudinal projection tract formation, we also included Hcrt neurons in our experiments. *robo2* transcripts are present in *otpb:gfp*-positive cells and in Hcrt neurons (data not shown).

To analyse mediolateral positioning of Hcrt axonal projections in comparison with *otpb:gfp*-positive projections, we used *otpb:gfp;hcrt:tdtomato* double transgenic zebrafish that were crossed into Robo2-deficient (ast^{ti272z}) mutants. In *ast* homozygous mutant embryos, we observed a significant medial displacement of HTS axons labelled by both transgenic lines when compared with heterozygous siblings (Fig. 3A-G; supplementary material Table S6). Thus, *otpb:gfp*-positive cells, as well as Hcrt neurons, require Robo2 for lateral positioning of HTS projection tracts.

Expression of *robo3a.1* is increased in *otpb:gfp*-positive neurons in the hypothalamus after *sim1a* or *arnt2* depletion

We next analysed the molecular mechanisms underlying the medial displacement of *otpb:gfp* HTS tracts in *sim1a* morphants and $arnt2^{hi2639}$ mutants. A previous study in mouse demonstrated that *Robo3* transcripts were upregulated in mammillary body neurons of $Sim1^{-/-}/Sim2^{-/-}$ double mutants (Marion et al., 2005). In zebrafish, two *robo3* isoforms (*robo3v1* and *robo3v2*) have been described, which only differ in a short stretch of amino acids at the N terminus (Challa et al., 2005). In accordance with the nomenclature of *Robo3* isoforms in mammals (Camurri et al., 2005; Chen et al., 2008), *robo3v2* will here be referred to as *robo3a.1*, and *robo3v1* as *robo3b.1*. Based on its specific and spatially restricted expression in the diencephalon, we focused on *robo3a.1* (Challa et al., 2005). To analyse expression of *robo3a.1* in relation to *otpb:gfp* neurons, we performed fluorescent in situ hybridization to *robo3a.1* in combination with anti-GFP immunohistochemistry. At 48 hpf, this analysis revealed a bilateral *robo3a.1* expression domain in the hypothalamus, which extends medially towards the midline. Based on *robo3a.1* and *otpb:gfp* expression profiles, the *robo3a.1* domain could be separated into an anterior (aH) and a

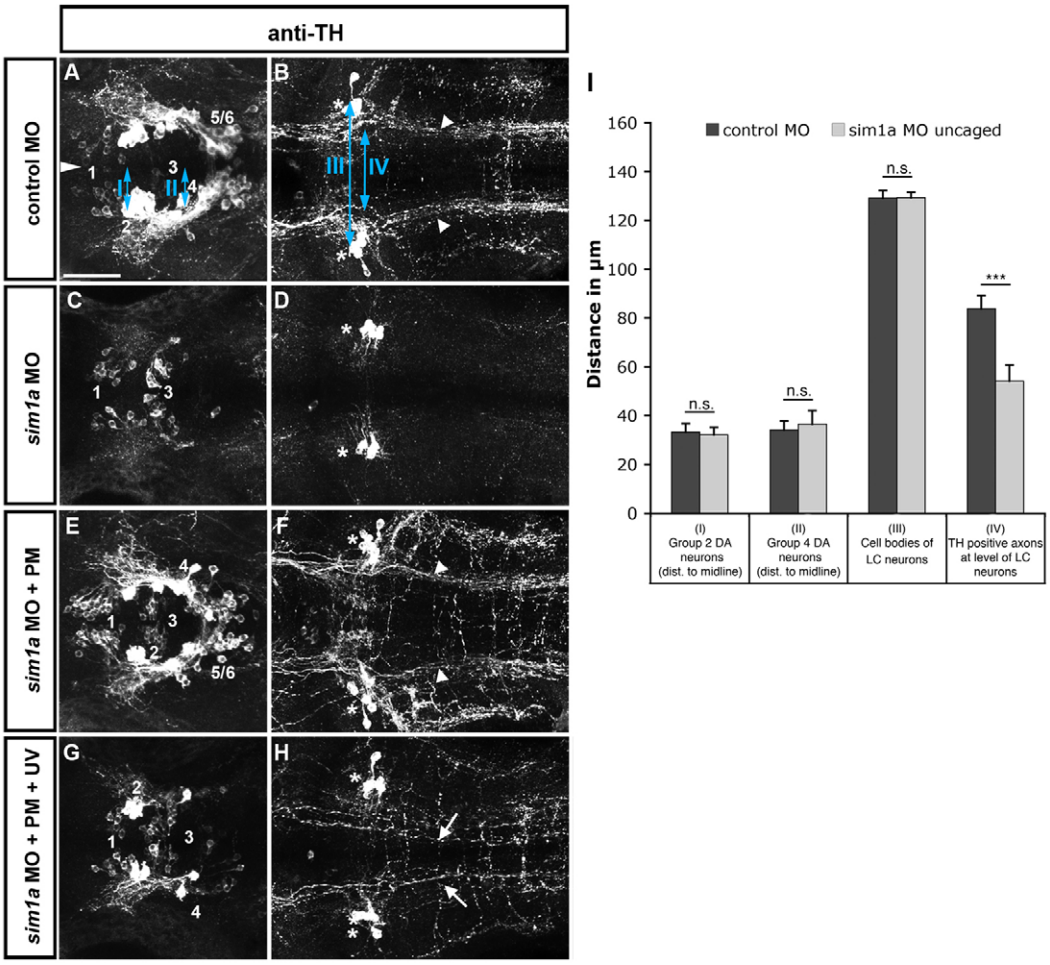

Fig. 2. Temporally controlled *sim1a* knockdown reveals medial displacement of dopaminergic longitudinal projection tracts. Dorsal views of confocal *z*-projections of 72 hpf embryos at the anterior-posterior levels of forebrain (A,C,E,G) and hindbrain (B,D,F,H). (**A**,**B**) Control MO injection. (**C**,**D**) *sim1a* morpholino injection: TH immunoreactivity is lost in cell bodies (C) and axons (D) of the DA HTS systems (DA groups 2,4-6). (**E**,**F**) Caging the *sim1a* morpholino results in wild-type-like formation of DA HTS systems. (**G**,**H**) Temporally controlled activation of *sim1a* MO at 22 hpf permits the formation of individual group 2,4-6 DA neurons (G) but causes a medial shift of TH-positive axons (arrows in H). Arrowheads in B indicate the position of TH-positive HTS tracts. Asterisks in B,D,F,H indicate TH-positive locus coeruleus (LC) neurons. Numbers in A,C,E,G indicate DA groups (Rink and Wullimann, 2002). (**I**) Quantification of mediolateral positioning of TH-positive HTS axons at 72 hpf at the level of LC neurons (IV in B)*;* of distances of group 2 (I in A) and group 4 cells (II in A) from the midline; and of distances between LC neurons (III in B). ***P<0.0001; n.s., not significant. Scale bar: 50 µm.

posterior (pH) part (Fig. 4G,J). In aH, *robo3a.1* is expressed only in a subset of GFP-positive cells at very low levels, whereas in pH, *robo3a.1* is co-expressed in most GFP-positive neurons (Fig. 4A-A′,D-D′). This expression profile coincides with the dynamic regulation of *robo3a.1* transcription during DA cell development (supplementary material Fig. S5).

We next evaluated *robo3a.1* expression in *otpb:gfp* transgenic *arnt2*^{hi2639} mutant embryos and in *otpb:gfp* embryos after *sim1a* MO knockdown (Fig. 4B-B′,C-C,E-E′,F-F,H,I). Our analysis reveals that, in response to *arnt2* or *sim1a* loss of function, *robo3a.1* expression levels are significantly increased in a subset of GFP neurons in the aH, whereas expression in pH was unchanged (Fig. 4K). By contrast, a change in expression levels of other Robo receptors or of Dcc was not detected (Fig. 4K and data not shown).

Taken together, these results provide evidence that *robo3a.1* transcription is dynamically regulated during development of *otpb:gfp* and DA neurons, and that Sim1a and Arnt2 transcription factors are required for downregulation of *robo3a.1* in aH as development proceeds.

Robo3 is required to define lateral positioning of *otpb:gfp*-positive longitudinal axons

We next tested a potential role of Robo3 during pathfinding of *otpb:gfp*-positive HTS longitudinal axons using Robo3 *twitch twice* (*twt*^{tw204}) mutants (Burgess et al., 2009). In *twt* mutant *otpb:gfp* embryos, the distance between longitudinal HTS axons in the hindbrain was significantly increased when compared with heterozygous siblings (Fig. 5A-E; supplementary material Table S7). In addition, we analysed pathfinding of Hcrt HTS axons, which do not express *robo3a.1* (supplementary material Fig. S6A-C). Formation of *hcrt:tdtomato*-positive longitudinal axons did not reveal a significant difference between *twt* mutant and heterozygous sibling embryos (supplementary material Fig. S6D-H, Table S7). Therefore, Robo3 function specifically contributes to mediolateral positioning of *otpb:gfp*-positive longitudinal axons but not of Hcrt axons.

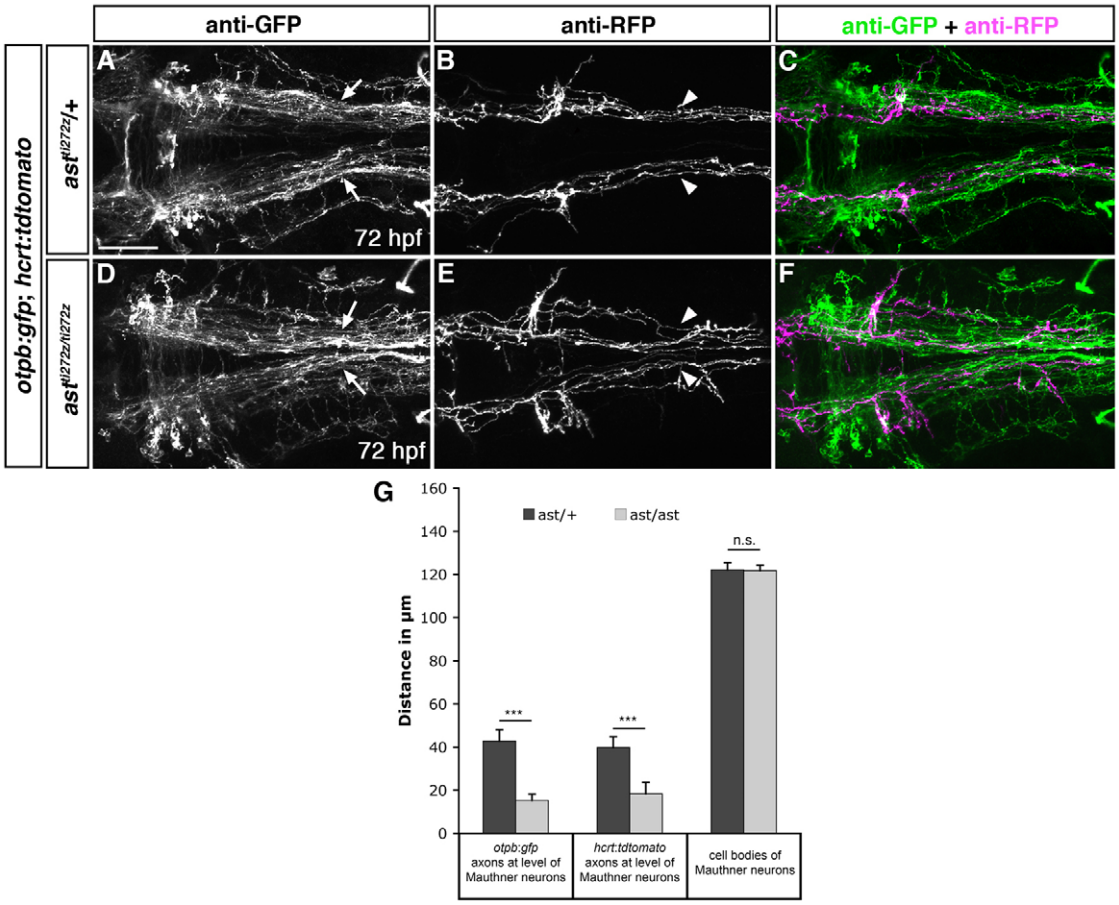

Fig. 3. Lateral positioning of longitudinal axons derived from *otpb*- and hypocretin-positive neurons is altered in *ast* homozygous mutants. Dorsal views of hindbrain confocal *z*-projections of *otpb:gfp;hcrt:tdtomato* double transgenic 72 hpf embryos. (**A**-**F**) In *ast/ast* embryos longitudinal projections of *otpb:gfp* (D,F; arrows in D) and *hcrt:tdtomato* (E,F; arrowheads in E) axons are shifted towards the midline compared with *ast*/+ siblings. (**G**) Quantification of the distance between *otpb:gfp* and *hcrt:tdtomato* HTS axons at the anterior-posterior level of Mauthner neurons, and of the distance between Mauthner neurons. ***P<0.0001; n.s., not significant. Scale bar in A for A-F: 50 µm.

Medial displacement of *otpb:gfp*- and TH-positive longitudinal axons after *sim1a* or *arnt2* depletion is suppressed in *robo3* mutants

To examine whether an increase of *robo3a.1* expression might be the cause for medial displacement of *otpb:gfp*-positive longitudinal axons, we assayed longitudinal tract formation after *sim1a* or *arnt2* knockdown in Robo3-deficient embryos. In *twt* heterozygous *otpb:gfp* embryos injected with *sim1a* MO, we observed a medial displacement of longitudinal axons. By contrast, this displacement upon *sim1a* knockdown was strongly attenuated in *twt* mutant *otpb:gfp* embryos (Fig. 5F-J; supplementary material Table S8). Knockdown of *arnt2* function resulted in similar findings (supplementary material Fig. S7A-E; Table S8). In order to demonstrate that negative regulation of *robo3* by Sim1a is required for the positioning of longitudinal DA tracts, we again used stage-specific knockdown of *sim1a* by photoactivation of morpholinos (supplementary material Fig. S8A-D). This analysis demonstrated a significant increase in the average distance of TH-positive longitudinal axons for *sim1a* photomorphants of *twt* mutant genotype when compared with *twt* heterozygous embryos (supplementary material Fig. S8E, Table S9). These two sets of experiments indicate that negative control of *robo3a.1* by Sim1a and Arnt2 is required for proper lateral positioning of *otpb:gfp* and DA longitudinal axons.

Overexpression of *robo3a.1* induces medial displacement of Robo2-dependent longitudinal axons

We next analysed whether mis-expression of *robo3a.1* was sufficient to induce medial displacement of Robo2-dependent longitudinal axons. In addition to *robo3a.1*, we also decided to analyse a potential role of *robo3b.1* in HTS formation. We analysed Otpb and Hcrt neurons, which require Robo2 function for longitudinal tract formation. To temporally control expression of *robo3a.1* or *robo3b.1*, we generated *hsp70l:robo3a.1* and *hsp70l:robo3b.1* transgenic lines, which enable comparable levels of ubiquitous *robo3a.1* or *robo3b.1* expression upon heat-shock treatment (data not shown). The heat-shock lines were crossed to the *otpb:gfp* and *hcrt:tdtomato* transgenic lines. Transgenic embryos were heat-induced (39°C for 50 minutes) at 24 and 28 hpf to maintain *robo3* expression during longitudinal HTS pathfinding. Heat-shock treatment did not affect formation of longitudinal axons in control or *hsp70l:robo3b.1* embryos. By contrast, mis-expression of *robo3a.1* resulted in medial displacement of longitudinal axons (Fig. 6). Quantification revealed a significant medial displacement phenotype after overexpression of *robo3a.1* when compared with controls or with overexpression of *robo3b.1* (Fig. 6G,N; supplementary material Tables S10, S11). In addition to the results

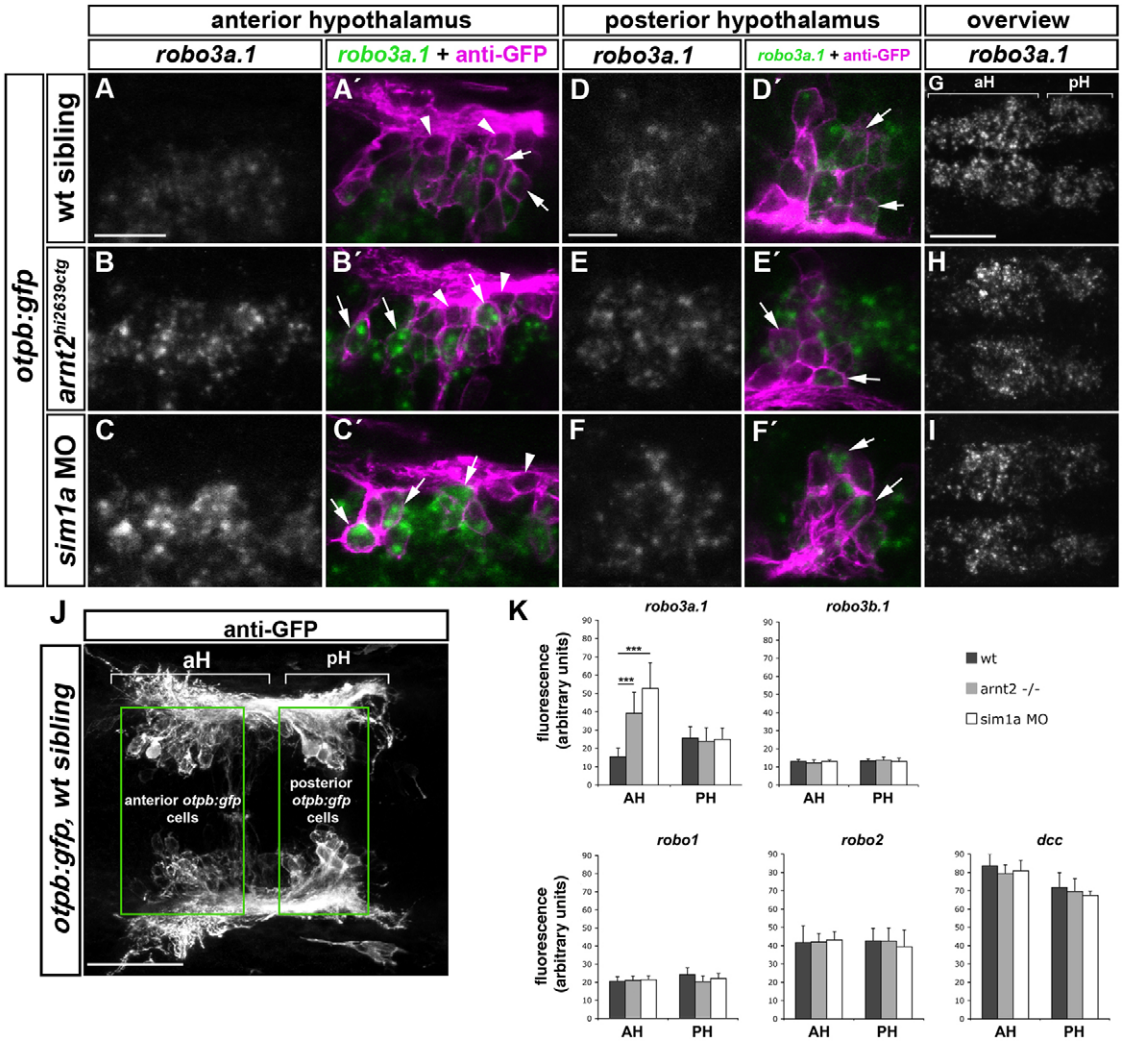

Fig. 4. Spatiotemporal expression of *robo3a.1* in the hypothalamus is altered in *sim1a* morphants and *arnt2* mutants. Dorsal views of confocal *z*-projections of 48 hpf embryos. Anterior is towards the left. (**A-F′**) High magnification of *otpb:gfp* cells in anterior (aH) or posterior hypothalamus (pH). (A,A′) Expression of *robo3a.1* is detected at low levels in a subset of GFP-positive cells (arrows in A′) in *otpb:gfp* embryos (B-C′). Instead, *otpb:gfp; arnt2*^{hi2639c} mutant embryos (B,B′) and *otpb:gfp* embryos injected with *sim1a* MO (C,C′) show strong *robo3a.1* signal in GFP-positive cells (arrows in B′ and C′). (D-F′) Expression levels of *robo3a.1* are comparable in GFP-positive cells in pH of *otpb:gfp* embryos (D,D′), *otpb:gfp; arnt2*^{hi2639c} mutants (E,E′) and *otpb:gfp* embryos injected with *sim1a* MO (F,F′). Arrowheads indicate GFP-positive cells, which do not express *robo3a.1*. (**G-I**) Overview of the *robo3a.1* expression domain in the hypothalamus of *otpb:gfp* embryos (G), *otpb:gfp; arnt2*^{hi2639c} mutant embryos (H) and *otpb:gfp* embryos injected with *sim1a* MO (I). (**J**,**K**) Quantification (K) of Alexa-488 signal intensity derived from fluorescent *in situ* hybridization staining for indicated genes in *otpb:gfp* cells located in aH or pH (J). ***P<0.0001. Scale bars: in A, 20 μm for A-C′; in D, 10 μm for D-F′; in G, 50 μm for G-I.

described above, we observed different phenotypes upon mis-expression of *robo3a.1* (enables midline crossing) and *robo3b.1* (prevents midline crossing) in commissural Mauthner neuron axons (J.S., unpublished).

Our findings demonstrate that mis-expression of *robo3a.1*, but not of *robo3b.1*, is sufficient to induce medial displacement of longitudinal HTS axons. Thus, the Robo3a.1 isoform is important for proper mediolateral positioning of HTS tracts.

Ectopic Robo3a.1 blocks Robo2-dependent repulsion

To analyse how ectopic *robo3a.1* expression may affect HTS tract formation, we first tested for a potential role of Robo3a.1 as a chemoattractive receptor. The medial displacement of DA longitudinal axons towards the midline in Robo2-deficient *ast* embryos can be rescued upon knockdown of attractive Dcc/Netrin signalling (Kastenhuber et al., 2009). If Robo3a.1 serves as an attractive receptor, we would predict that a combined knockdown of *sim1a* (thereby increasing Robo3a.1) and *dcc* (thereby removing Dcc-mediated attraction) should still result in medial displacement phenotype of *otpb:gfp* HTS axons. However, we found that medial displacement of longitudinal axons was significantly reduced following co-injection of *sim1a* MO and *dcc* MO when compared with controls (Fig. 7A-E; supplementary material Table S12). This indicates that attraction mediated by Dcc causes medial displacement of longitudinal axons after *sim1a* knockdown, and argues against a role of Robo3a.1 as an attractive receptor.

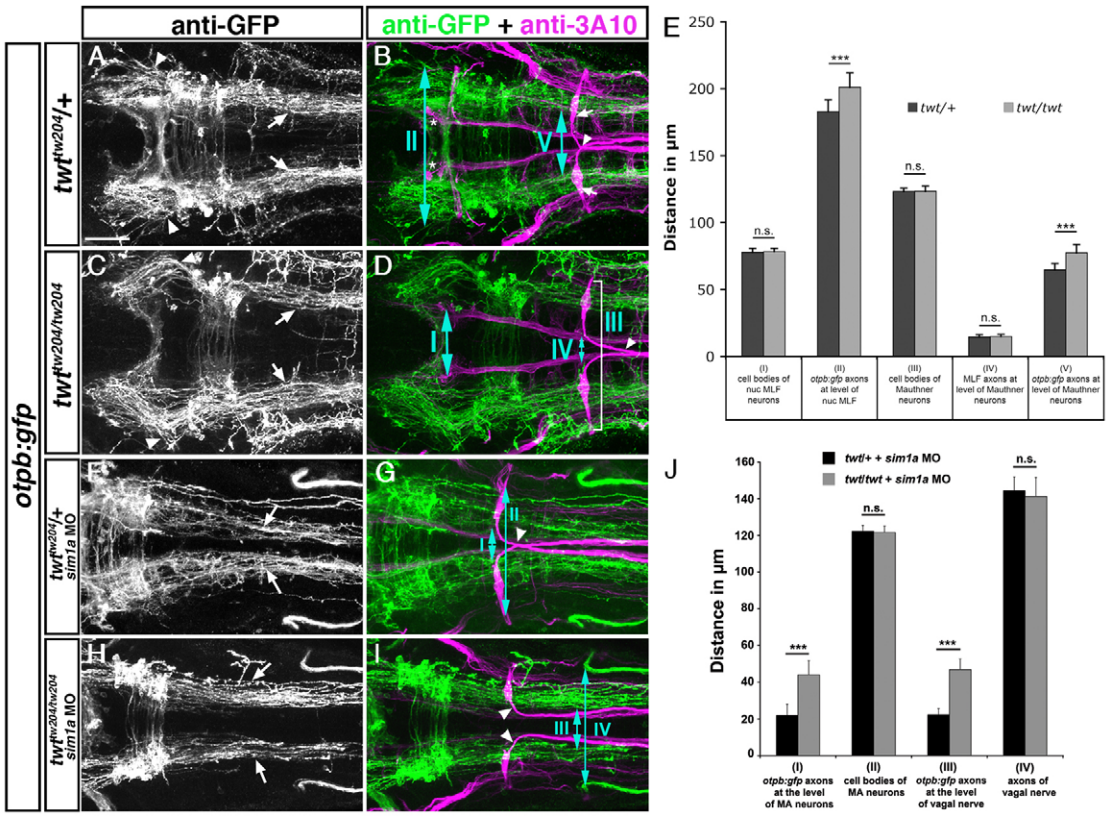

Fig. 5. Robo3 is required for lateral positioning of *otpb:gfp*-positive longitudinal axons. Dorsal views of confocal hindbrain *z*-projections (72 hpf) are shown. Anterior is towards the left. (**A**,**B**) In *twt*/+ embryos, *otpb:gfp* longitudinal axons in the midbrain (A, arrowheads) and hindbrain (A, arrows) grow by a defined distance towards the midline. Arrows in B indicate Mauthner neuron somata. (**C**,**D**) In *twt/twt* embryos, *otpb:gfp* longitudinal axons project more laterally in the midbrain (C, arrowheads) and hindbrain (C, arrows). (**E**) Quantification of the separation between *otpb:gfp* longitudinal axons in mid- and hindbrain (double-headed arrows, II and V in B) and between nucMLF somata (I, see asterisks in B), MLF axons (IV) or MA neurons (III) in *twt*/+ or *twt/twt* embryos. (**F**,**G**) In *sim1a* MO-injected *twt*/+ embryos, *otpb:gfp* longitudinal axons are medially displaced (F, arrows). (**H**,**I**) In *sim1a* MO-injected *twt/twt* embryos, *otpb:gfp* longitudinal axons project more laterally (H, arrows). (**J**) Quantification of the distance between MA neurons (II, marked in G) and vagal axons (IV in H), or of the distance between *otpb:gfp* longitudinal axons (I in H and III in G) in *sim1a* MO-injected *twt*/+ and *twt/twt* embryos. Arrowheads in B,D,G,I indicate pathfinding of Mauthner neurons in *twt*/+ and *twt/twt* embryos. **P*<0.001. Scale bar: 50 µm.

We next analysed whether Robo3a.1 interferes with repulsion by Robo2 as suggested previously (Chen et al., 2008). If Robo3a.1 compromised Robo2 repulsion, then increased levels of *robo3a.1* in the *ast* mutant background should not lead to a stronger medial displacement phenotype. Quantification of medial displacement of longitudinal axons after depletion of *sim1a* in *ast/ast*;*twt*/+ embryos (increased *robo3a.1* expression), and in *ast; twt* double mutant embryos (no *robo3a.1* expression) compared with *ast/ast; twt/twt* double mutants injected with control MO revealed similar phenotypic strength (Fig. 8A-G; supplementary material Table S13).

To further support these findings, we made use of two different *ast*/*robo2* alleles, the strong ast^{ti272z} and the weaker ast^{te284} allele (Chalasani et al., 2007; Fricke et al., 2001). Consistently, the medial displacement phenotype of HTS axons is less pronounced in the weak *ast* mutants (Fig. 9A,J,I,R). We hypothesised that residual Robo2 signalling in weak *ast* embryos should be rendered less effective after *robo3a.1* mis-expression. If so, the resulting reduced effectiveness of Robo2 signalling would be predicted to increase HTS medial displacement in weak, but not strong, *ast* mutants. The experiment showed that the medial displacement phenotype was not increased upon overexpression of *robo3a.1* in the strong *ast* mutants. By contrast, a significant increase in medial displacement phenotype was observed after overexpression of *robo3a.1* in the weak *ast* mutant background (Fig. 9; supplementary material Table S14). Taken together, these results are consistent with Robo3a.1 functioning to attenuate repulsion by Robo2, and that attraction by Dcc then directs longitudinal axons towards the midline.

The extracellular N-terminal domain present in the Robo3a.1 isoform is important for interfering with Robo2-dependent repulsion

To identify structural characteristics of Robo3 isoforms required for interference with Robo2-dependent repulsion, we used the Gal4/UAS system for Hcrt-specific expression of different *robo3* isoforms together with *tdtomato*. A *hcrt:gal4* driver was co-injected with *UAS:robo3-P2A-tdtomatoCAAX* responders harbouring different Robo3 isoforms, and embryos showing transient expression of the tdTomato reporter were analysed. Whole-mount *in situ* hybridization for *tdtomato* revealed similar expression levels for the different *robo3* isoforms (supplementary material Fig. S9). The medial displacement phenotype was quantified when tdTomato-positive longitudinal axons were in close contact with 3A10-positive MLF axons (Fig. 10C,D). All midline crossing events caudal to the

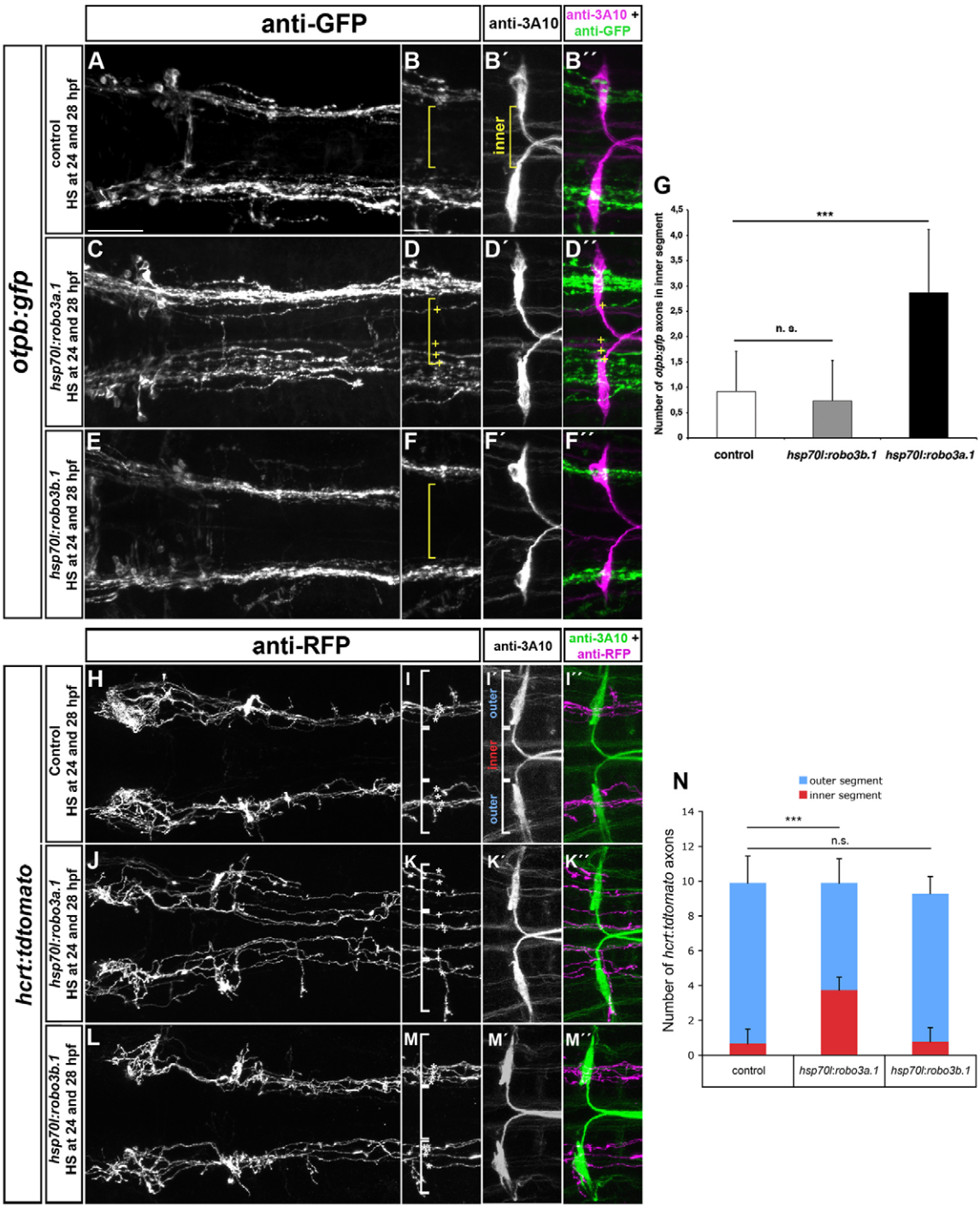

Fig. 6. Ectopic expression of *robo3a.1* is sufficient to induce medial displacement of HTS axons. (A-F″,H-M″) Dorsal views of confocal *z*-projections of brain regions of 48 hpf (A-F″) and 72 hpf (H-M″) embryos. Anterior is towards the to left. (**A-B″**,**H-I″**) Heat-shock treatment does not affect pathfinding of *otpb:gfp* or *hcrt:tdtomato* longitudinal axon in control embryos. (**C-D″**,**J-K″**) Longitudinal *otpb:gfp* or *hcrt:tdtomato* axons are medially displaced after heat shock-induced overexpression of *robo3a.1*. (**E-F″**,**L-M″**) Pathfinding of *otpb:gfp* or *hcrt:tdtomato* longitudinal axons is normal after overexpression of *robo3b.1*. (**G**,**N**) Quantification of the number of *otpb:gfp* or *hcrt:tdtomato* longitudinal axons in defined outer or inner sections. Brackets in B,B′,D,F, I,I′,K,M, indicate outer and inner sections as defined by Mauthner neuron somata (outer section) and the area in between (inner section) used for quantification. Asterisks and plus signs indicate longitudinal HTS axons in outer and inner sections, respectively. Scale bars: in A, 50 μm for A,C,E,H,J,L; in B, 25 μm for B-B″,D-D″,F-F″,I-I″,K-K″,M-M″.

level of the nucMLF were considered to be ectopic (Fig. 10C). Expression of tdTomato alone or of *robo3b.1* in Hcrt neurons did not affect longitudinal tract formation. By contrast, mis-expression of *robo3a.1* resulted in medial displacement of longitudinal axons and ectopic midline crossing events (Fig. 10A-F,K; supplementary material Table S15). To analyse requirement of Robo3A cytoplasmatic domains, we mis-expressed mouse *Robo3A.1* and *Robo3A.2* in Hcrt neurons. The two mouse Robo3A isoforms encode

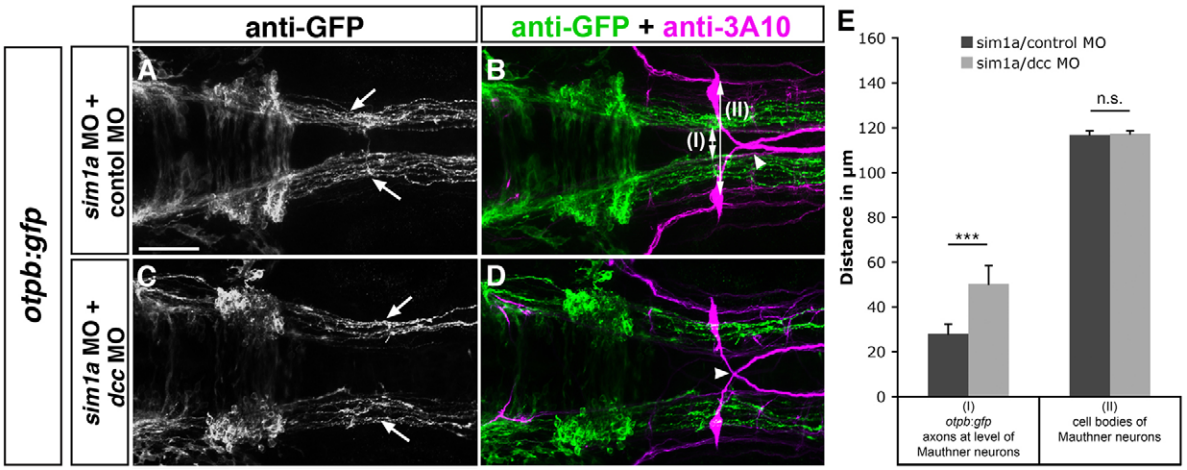

Fig. 7. Dcc-mediated attraction causes medial displacement of *otpb:gfp* longitudinal axons after *sim1a* knockdown. Dorsal views of hindbrain confocal *z*-projections of 48 hpf *otpb:gfp* embryos. Anterior is towards the left. (**A-D**) GFP-positive longitudinal axons are medially displaced towards the midline (A, arrows) after co-injection of *sim1a* MO and control MO in *otpb:gfp* embryos. Medial displacement of longitudinal *otpb:gfp* axons (C, arrows) is reduced after combined injection of *sim1a* MO and *dcc* MO. (**E**) Quantification of the distance between *otpb:gfp*-positive longitudinal axons (I) or of the distance between Mauthner neurons (II) of indicated treatments. Arrowheads in B,D indicate normal midline crossing of MA neurons. **P*<0.001; n.s., not significant. Scale bar: 50 µm.

a similar N-terminus to zebrafish *robo3a.1*, but distinct C termini and contribute to different aspects of commissural axon guidance (Chen et al., 2008). Similar to our findings upon mis-expression of zebrafish *robo3a.1*, mis-expression of mouse *Robo3A.1* or *Robo3A.2* resulted in medial displacement of longitudinal axons and ectopic midline crossing (Fig. 10G-J,K; supplementary material Table S15).

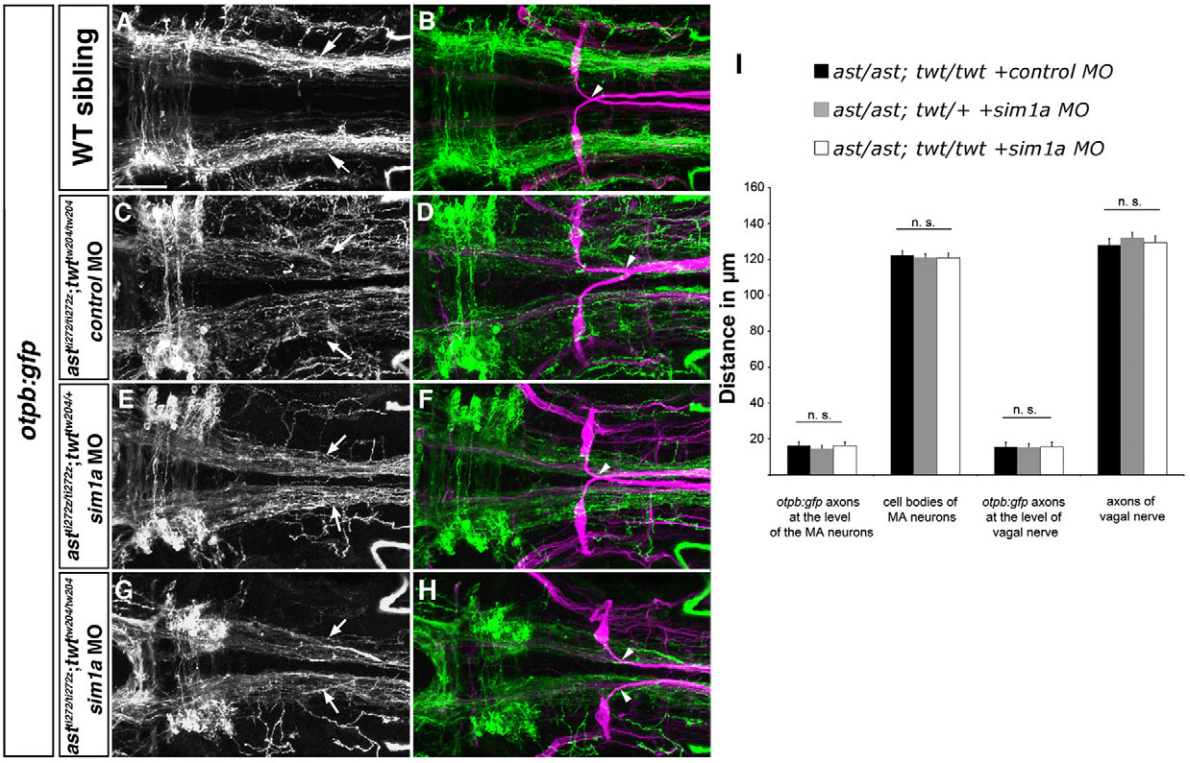

Fig. 8. Medial displacement phenotype of *otpb:gfp* longitudinal HTS axons is not affected by depletion of *sim1a* in *ast/ast; twt/+* and *ast/ast; twt/twt* embryos. Dorsal views of hindbrain confocal *z*-projections of 72 hpf *otpb:gfp* embryos. Anterior is towards the left. (**A**,**B**) *otpb:gfp* HTS axons (arrows) in a wild-type sibling. (**C-H**) Phenotypic strength of medial displacement of *otpb:gfp*-positive longitudinal axons is similar in *ast/ast; twt/twt* embryos injected with control MO (C, arrows), and in *ast/ast*; *twt/+* (E, arrows) or *ast/ast; twt/twt* (G, arrows) *sim1a* morphant embryos. Arrowheads in B,D,F,H indicate pathfinding of Mauthner neurons. (**I**) Quantification of the distance between of *otpb:gfp* longitudinal axons and vagal axons, and of the distance between Mauthner neurons in *ast/ast; twt/twt* embryos injected with control MO, and in *ast/ast; twt/+* or *ast/ast; twt/twt* embryos injected with *sim1a* MO. n.s., not significant. Scale bar: 50 µm.

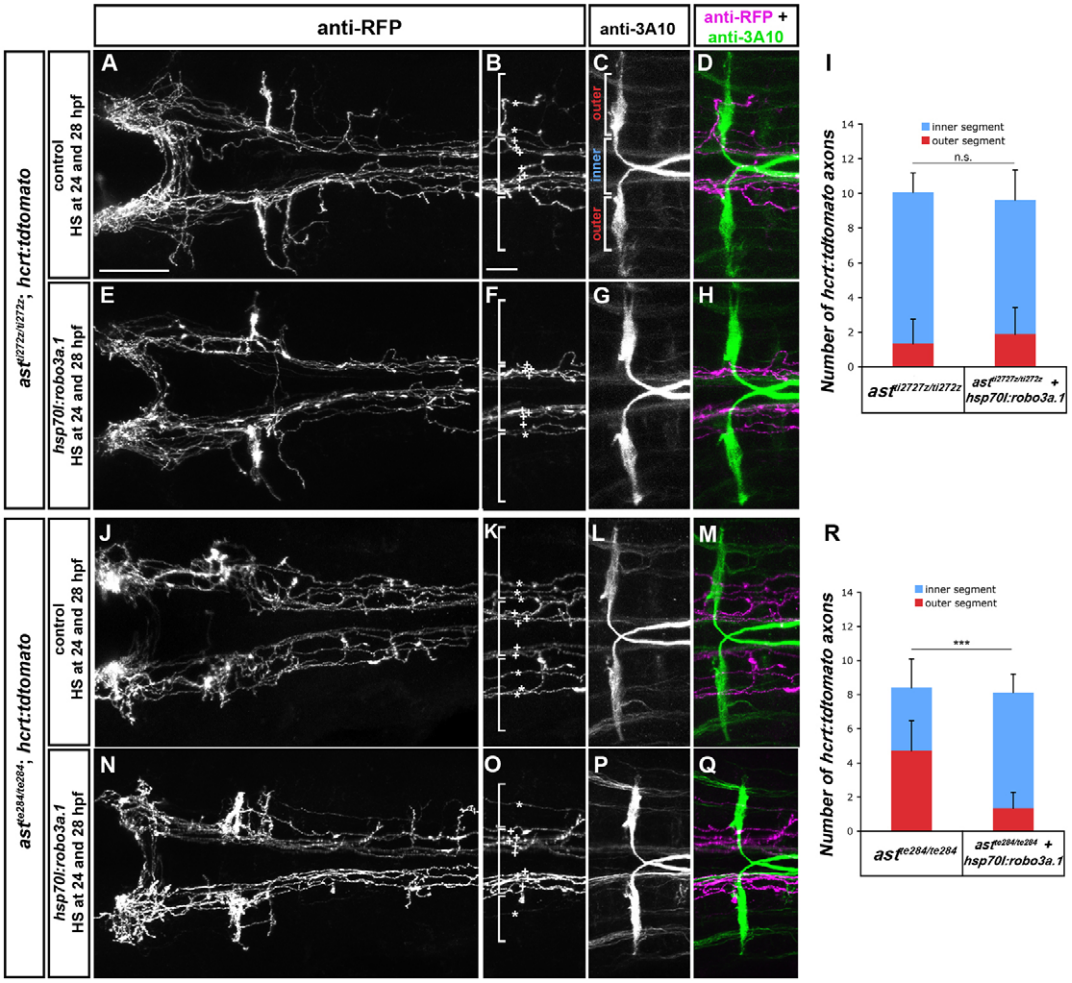

Fig. 9. Overexpression of *robo3a.1* leads to increased medial displacement of longitudinal HTS axons in *ast*^{te284} but not in *ast*^{ti272z} embryos. Dorsal views of confocal *z*-projections of the brain and hindbrain of 72 hpf *hcrt:tdtomato* embryos. Anterior is towards the left. (**A-H**) Medial displacement phenotype of *hcrt:tdtomato* HTS axons is similar in *ast*$^{ti272z/ti272z}$ and *ast*$^{ti272z/ti272z}$*; hsp70l:robo3a.1* embryos after heat-shock treatment. (**J-Q**) Medial displacement phenotype of *hcrt:tdtomato* HTS axons is increased in *ast*$^{te284/te284}$*; hsp70l:robo3a.1* embryos when compared with *ast*$^{te284/te284}$ embryos. (**I**,**R**) Quantification of the number of *hcrt:tdtomato* longitudinal axons in outer or inner sections in *ast*^{ti272z} (I) or *ast*^{te284} (R). Brackets in B,C,F,K,O indicate outer and inner sections used for quantification, defined by Mauthner neuron somata (outer section) and the area in between (inner section). Asterisks and plus signs indicate longitudinal *hcrt:tdtomato* axons in outer and inner sections, respectively. Scale bars: in A, 50 μm for A,E,J,N; in B, 25 μm for B-D,F-H,K-M,O-Q.

Taken together, our results show that ectopic expression of zebrafish *robo3a.1* and mouse *Robo3A.1* or *Robo3A.2* isoforms is sufficient to induce medial displacement of Robo2-dependent longitudinal axons. This suggests that blocking of Robo2 activity primarily occurs via the specific N-terminal domain present in the Robo3A isoforms.

DISCUSSION

Our data reveal a novel function for Arnt2 and Sim1a transcription factors in establishment of HTS longitudinal axon tracts. Arnt2 and Sim1 are key regulators for differentiation of at least five different neuroendocrine cell lineages and of A11-related DA neurons in the hypothalamus (Löhr et al., 2009; Michaud et al., 2000; Michaud et al., 1998). As these diverse neuronal types all develop descending projections to the spinal cord, we analysed whether Sim1a and Arnt2 would contribute to control of axonal pathfinding. We found that loss of Arnt2 or Sim1a function results in a medial shift of HTS trajectories while passing the hindbrain. Our data reveal that Sim1a and Arnt2 negatively regulate expression of *robo3a.1*, a specific *robo3* isoform, which in turn inhibits Robo2 signalling activity.

In mouse embryos that lack Sim1 and/or Sim2 function, projection behaviour of hypothalamic neurons of the mammillary body is altered, resulting in aberrant midline crossing (Marion et al., 2005). These findings indicate that Sim transcription factor function may contribute to axon pathfinding for diverse neural populations. By contrast, Arnt2 function has been reported to be dispensable in this system. Our data indicate that *sim1a* and *arnt2*, similar to their role during neuronal differentiation (Michaud et al., 2000), act synergistically during HTS axon guidance. *Robo3* transcripts have been reported to be upregulated in the mammillary body of *Sim1*$^{-/-}$*/Sim2*$^{-/-}$ double mutants, suggesting that Robo3 might contribute to the reported axon guidance defects (Marion et al., 2005). Our analysis of HTS tract formation reveals similar mechanisms for Sim1a and Arnt2, and elucidates for both factors downstream molecular

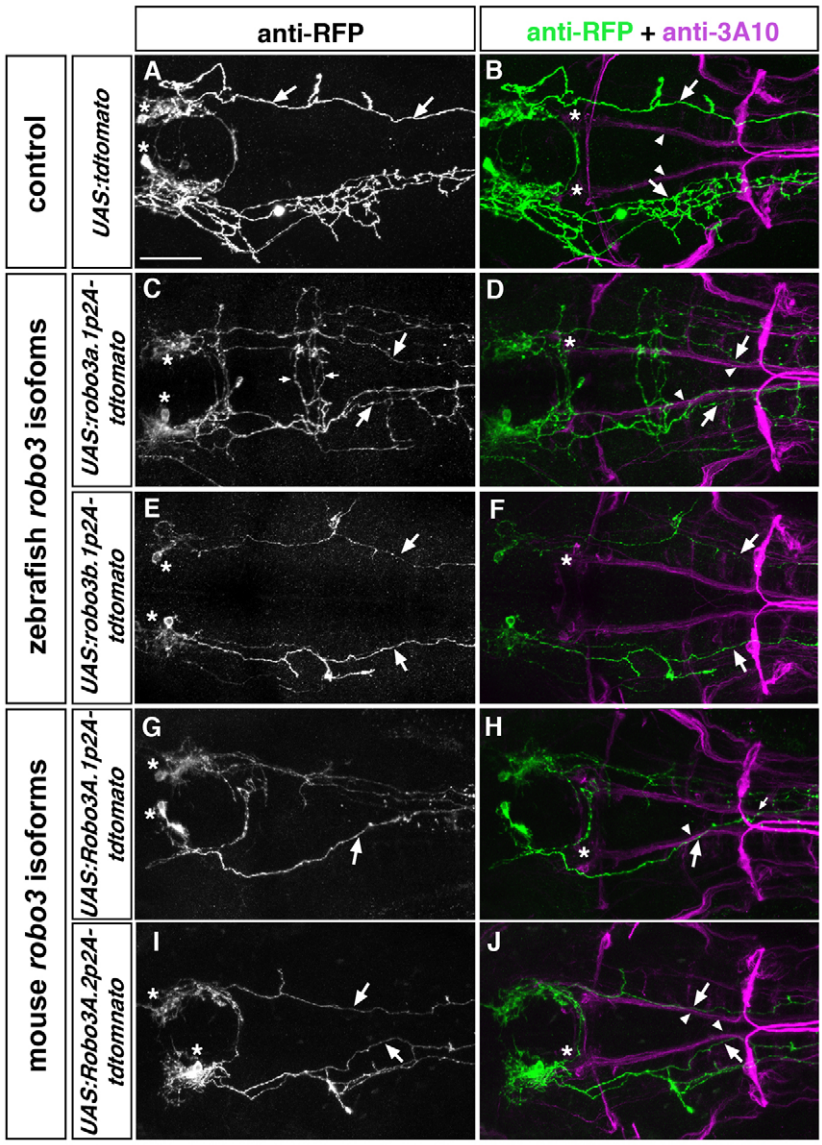

K

	Embryos	(%) Midline displacement	(%) Midline crossing
UAS:tdtomato	22	16.2	11.1
UAS:robo3a.1p2Atdtomato	23	78.2	52.2
UAS:robo3b.1p2Atdtomato	21	14.2	14.2
UAS:Robo3A.1p2Atdtomato	20	55	30
UAS:Robo3A.2p2Atdtomato	21	42.8	23.8

Fig. 10. The N-terminal domain present in Robo3A isoforms is important for interfering with Robo2-dependent repulsion. Dorsal views of hindbrain confocal *z*-projections of 72 hpf embryos. Anterior is towards the left. Embryos were co-injected with *hcrt:gal4* and UAS constructs indicated on the left. (**A**,**B**) Hcrt neurons form tdTomato-positive longitudinal axons (A, arrows), which project laterally (B, arrows) to the MLF (B, arrowheads). (**C**,**D**) After mis-expression of *robo3a.1* in Hcrt neurons, tdTomato-positive longitudinal axons are medially displaced towards the midline (C,D, arrows) and project together with the medial longitudinal fascicle (D, arrowheads). Small arrows indicate ectopic midline crossing events (C). (**E**,**F**) Upon mis-expression of *robo3b.1* in Hcrt neurons, tdTomato-positive longitudinal axons project normally (E,F, arrows). (**G-J**) After mis-expression of mouse *Robo3A.1* (G,H) or *Robo3A.2* (I,J) in Hcrt neurons, tdTomato-positive longitudinal axons are displaced towards the midline (G-J, arrows) and project together with the medial longitudinal fascicle (H,J, arrowheads). Small arrow in H indicates midline crossing. (**K**) Quantification. Asterisks in A,C,E,G,I indicate Hcrt neurons, asterisks in B,D,F,H,J indicate nucMLF neurons. Scale bar: 50 μm.

mechanisms affecting axon guidance. However, mediolateral positioning of HTS axons is not completely restored upon depletion of *sim1a* or *arnt2* in *robo3* mutant embryos, suggesting additional HTS axon guidance control mechanisms by Sim1a and Arnt2. Downstream targets of Sim1 and Arnt2 include transcriptional regulators, as well as cell migration-related genes (Liu et al., 2003), which may contribute to HTS axon guidance independent of Robo3. In *Drosophila*, abrogation of *sim* leads to an axonal fasciculation phenotype (Freer et al., 2011), which differs from the mouse *Sim1* or zebrafish *sim1a* loss-of-function defects. Thus, Sim1 may control different aspects of axonal pathfinding by regulating different axon guidance factors.

How does upregulated *robo3a.1* misguide pathfinding of HTS longitudinal axons? Previous work suggested that Robo3a.1 may inactivate Robo1 and Robo2 receptors and thereby render pre-crossing commissural axons unresponsive to Slit repulsion (Chen et al., 2008). Several observations argue that a similar mechanism between Robo3A.1 and Robo2 may lead to the medial displacement phenotype of HTS longitudinal axons. The *sim1a* or *arnt2* loss-of-function axon tract phenotypes share many features with Robo2 mutants. These similarities suggest that Robo3A.1 interferes with Robo2 activity. This notion is further strengthened by our findings that increased activity of Robo3a.1 (by either *sim1a* depletion or *robo3a.1* overexpression) enhances the medial displacement phenotype of HTS axons in weak, but not strong, *ast* mutants. These genetic experiments reveal that Robo3 acts only through Robo2 in this developmental context, but has no Slit-dependent signalling activity independent of Robo2. This indicates that Robo3A.1 does not serve as an attractive receptor. Furthermore, our observations after combined knockdown of *sim1a*

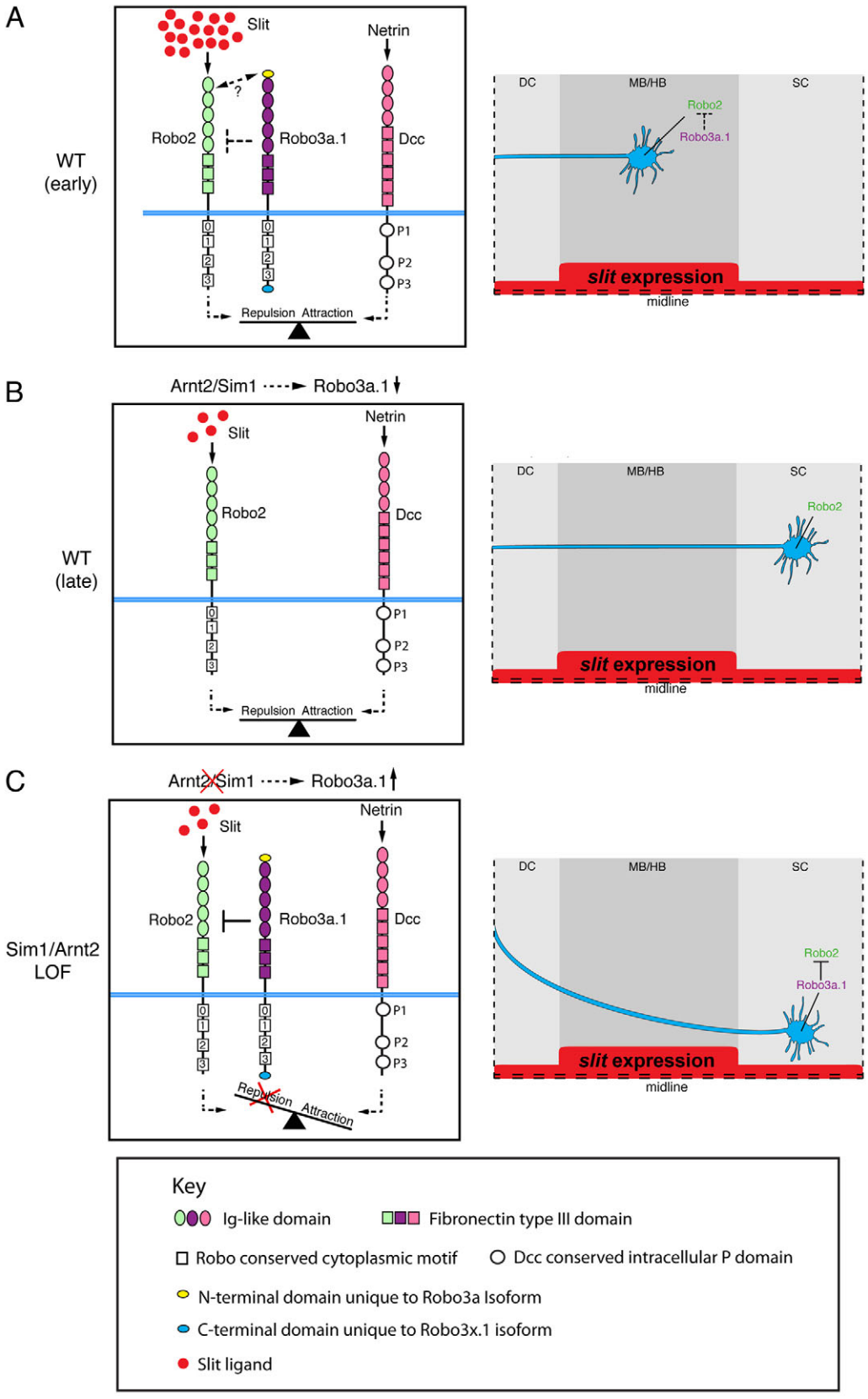

Fig. 11. Model for control of Robo2 activity during longitudinal HTS pathfinding. (**A**) During early stages, Robo3a.1 reduces repulsive activity of Robo2, while HTS axons navigate through areas of high *slit* expression levels in mid- and hindbrain. Double-headed arrow indicates potential Robo2/Robo3a.1 interaction domains. (**B**) Sim1a and Arnt2 negatively regulate *robo3a.1* at later stages when HTS axons have passed regions of high *slit* expression. Lateral positioning in the spinal cord is then controlled by full activity of Robo2/Slit signalling. (**C**) Model of abnormal HTS axon trajectories in Arnt2 and Sim1a loss-of-function embryos: 'attenuation' of Robo/Slit signalling activity persists when axons travel through hindbrain because Robo3a.1 downregulation fails to occur after Arnt2/Sim1a depletion. As a result, HTS axons receive less Robo/Slit signalling activity and are medially displaced. For conserved Robo3 domains, see key. DC, diencephalon; MB/HB, midbrain-hindbrain; sc, spinal cord.

and *dcc* suggest that attraction mediated by Dcc is the driving force that directs *otpb:gfp* longitudinal axons towards the midline. This finding relates to our previous results demonstrating that knockdown of *dcc* in *ast* mutants restores mediolateral positioning of DA longitudinal axons (Kastenhuber et al., 2009). Our data indicate that Robo3a.1 inhibits Robo2-mediated repulsion and that attraction by Dcc then directs HTS longitudinal axons towards the midline.

How does Robo3A.1 interfere with Robo2 activity? Our results on the mis-expression of different combinations of N- and C-terminal zebrafish and mouse Robo3a and Robo3b isoforms in Hcrt neurons suggest that the N-terminal domain present in Robo3A is important for inhibiting Robo2 activity during HTS axon guidance. A recent study demonstrated that different C-terminal domains present in mouse Robo3A.1 and Robo3A.2 contribute to distinct aspects of commissural axon guidance (Chen et al., 2008). Robo3A.1 allows midline crossing by potentially blocking activity of Robo1 and Robo2, whereas Robo3A.2 may prevent re-crossing by collaboration with Robo1 and Robo2. How can the observed differences be explained? Commissural and ipsilateral axon guidance mechanisms use similar sets of guidance cues, but respond with different projections (for a review, see Evans and Bashaw, 2010a). Thus, it is conceivable that DA and *otpb:gfp*-positive longitudinal growth cones, in contrast to commissural neurons, use a distinct pathway involving solely the N-terminal domain found in Robo3A isoforms to attenuate Robo2 activity. In *Drosophila*, different functions of Robo2 and Robo3 are specified by their ectodomains, and do not reflect differences in cytoplasmic signalling (Evans and Bashaw, 2010b; Spitzweck et al., 2010). Alternatively, as we failed to identify different C-terminal *robo3* isoforms in zebrafish (data not shown), it is also possible that zebrafish solely use the N-terminal Robo3a.1 and Robo3b.1 isoforms to control different aspects of axon guidance. In addition to the results presented here, a role for Robo3a.1 and Robo3b.1 during axon guidance, has also been suggested by others (Challa et al., 2005; Devine and Key, 2008). Our findings indicate that inhibition of Robo2 activity via the N-terminal domain present in Robo3A isoforms occurs extracellularly during pathfinding of HTS axons. However, the precise molecular interactions remain elusive. The Robo3A specific domain could interfere with Robo2 by direct physical interaction, and thereby mask the Slit-binding domain of Robo2 mapped within the immunoglobulin-like domains 1 and 2 (Hohenester, 2008). Alternatively, repulsion by Robo2 may be inhibited by ectodomain-dependent heterodimerisation of Robo3A.1 and Robo2 in a Slit-independent fashion, similar to findings in *Drosophila* (Evans and Bashaw, 2010b).

What is the role of Robo3A.1 during longitudinal pathfinding? Lateral positioning of longitudinal axons is primarily governed by repulsion through midline derived Slit proteins (Farmer et al., 2008; Kastenhuber et al., 2009). In zebrafish, the four known Slit genes display strong expression at the midline of the midbrain and hindbrain, and lower expression within the spinal cord, suggesting different Slit levels (supplementary material Fig. S10) (Hutson et al., 2003; Yeo et al., 2001). Therefore, in order to maintain constant mediolateral positioning in regions with different Slit levels, the growth cones of DA and *otpb:gfp*-positive longitudinal axons may have adopted a mechanism to modulate Slit-dependent repulsion from the midline (Fig. 11). Robo3A.1 may contribute to this mechanism by reducing the activity of Robo2 and thus attenuating repulsion by Slit proteins. The Robo3A.1 dependent 'attenuation' mechanism may then enable the navigation of longitudinal *otpb:gfp* or DA growth cones to keep lateral positioning in the mid- and hindbrain despite high expression levels of *slits* (Fig. 11A,A′). Sim1a and Arnt2 contribute to this mechanism by controlling negative regulation of *robo3a.1* in a stage-dependent manner synchronized with progress of axonogenesis. Complete downregulation of *robo3a.1* then leads to full activation of Robo2, which allows for proper lateral positioning within the lower *slit* levels expressed in the spinal cord (Fig. 11B,11B′). In *arnt2* or *sim1a* loss-of-function embryos, stage-dependent negative control of *robo3a.1* does not occur. Therefore, Robo3a.1 is still present and inhibits Robo2 activity when longitudinal axons approach the spinal cord. When Robo2 activity is severely attenuated by Robo3a.1 overexpression, repulsion and attraction are imbalanced and longitudinal growth cones are directed towards the midline by Dcc/Netrin-mediated attraction (Fig. 11C,11C′).

In summary, we have shown that Arnt2 and Sim1a transcription factors contribute to proper positioning of HTS longitudinal axon tracts. Sim1a and Arnt2 perform this function by negative regulation of *robo3a.1* transcription at a specific stage of neuroendocrine and DA cell differentiation. Precise control of *robo3a.1* expression is essential for proper longitudinal tract formation, as Robo3A.1 attenuates Robo2 activity to adjust lateral positioning within different Slit levels. Thus, our findings reveal a novel mechanism to ensure correct lateral positioning of longitudinal projections navigating through changing signalling environments.

Acknowledgements
We thank C. Beattie and M. Tessier-Lavigne for *robo3* cDNAs, P. Mourrain for the *hcrt* promoter and M. Hammerschmidt for sharing unpublished results. We thank the zebrafish community for sharing reagents and S. Götter for expert zebrafish care. We thank Virginie Lecaudey, Erin Beddows, Marcus Frank and Jochen Holzschuh for comments on the manuscript.

Funding
This work was supported by the German Research Foundation [DFG-SFB780-B6 to W.D. and DFG-SCHW1404/1-1 to J.S.) and by the European Commission (FP7, mdDANEURODEV, to W.D.).

Competing interests statement
The authors declare no competing financial interests.

Supplementary material
Supplementary material available online at
http://dev.biologists.org/lookup/suppl/doi:10.1242/dev.087825/-/DC1

References

Acampora, D., Postiglione, M. P., Avantaggiato, V., Di Bonito, M., Vaccarino, F. M., Michaud, J. and Simeone, A. (1999). Progressive impairment of developing neuroendocrine cell lineages in the hypothalamus of mice lacking the Orthopedia gene. *Genes Dev.* **13**, 2787-2800.

Björklund, A. and Skagerberg, G. (1979). Evidence for a major spinal cord projection from the diencephalic A11 dopamine cell group in the rat using transmitter-specific fluorescent retrograde tracing. *Brain Res.* **177**, 170-175.

Blechman, J., Borodovsky, N., Eisenberg, M., Nabel-Rosen, H., Grimm, J. and Levkowitz, G. (2007). Specification of hypothalamic neurons by dual regulation of the homeodomain protein Orthopedia. *Development* **134**, 4417-4426.

Borodovsky, N., Ponomaryov, T., Frenkel, S. and Levkowitz, G. (2009). Neural protein Olig2 acts upstream of the transcriptional regulator Sim1 to specify diencephalic dopaminergic neurons. *Dev. Dyn.* **238**, 826-834.

Brose, K., Bland, K. S., Wang, K. H., Arnott, D., Henzel, W., Goodman, C. S., Tessier-Lavigne, M. and Kidd, T. (1999). Slit proteins bind Robo receptors and have an evolutionarily conserved role in repulsive axon guidance. *Cell* **96**, 795-806.

Burgess, H. A., Johnson, S. L. and Granato, M. (2009). Unidirectional startle responses and disrupted left-right co-ordination of motor behaviors in robo3 mutant zebrafish. *Genes Brain Behav.* **8**, 500-511.

Butler, S. J. and Tear, G. (2007). Getting axons onto the right path: the role of transcription factors in axon guidance. *Development* **134**, 439-448.

Camurri, L., Mambetisaeva, E., Davies, D., Parnavelas, J., Sundaresan, V. and Andrews, W. (2005). Evidence for the existence of two Robo3 isoforms with divergent biochemical properties. *Mol. Cell. Neurosci.* **30**, 485-493.

Chalasani, S. H., Sabol, A., Xu, H., Gyda, M. A., Rasband, K., Granato, M., Chien, C. B. and Raper, J. A. (2007). Stromal cell-derived factor-1 antagonizes slit/robo signaling *in vivo*. *J. Neurosci.* **27**, 973-980.

Challa, A. K., McWhorter, M. L., Wang, C., Seeger, M. A. and Beattie, C. E. (2005). Robo3 isoforms have distinct roles during zebrafish development. *Mech. Dev.* **122**, 1073-1086.

Chen, Z., Gore, B. B., Long, H., Ma, L. and Tessier-Lavigne, M. (2008). Alternative splicing of the Robo3 axon guidance receptor governs the midline switch from attraction to repulsion. *Neuron* **58**, 325-332.
Del Giacco, L., Sordino, P., Pistocchi, A., Andreakis, N., Tarallo, R., Di Benedetto, B. and Cotelli, F. (2006). Differential regulation of the zebrafish orthopedia 1 gene during fate determination of diencephalic neurons. *BMC Dev. Biol.* **6**, 50.
Devine, C. A. and Key, B. (2008). Robo-Slit interactions regulate longitudinal axon pathfinding in the embryonic vertebrate brain. *Dev. Biol.* **313**, 371-383.
Dugan, J. P., Stratton, A., Riley, H. P., Farmer, W. T. and Mastick, G. S. (2011). Midbrain dopaminergic axons are guided longitudinally through the diencephalon by Slit/Robo signals. *Mol. Cell. Neurosci.* **46**, 347-356.
Eaton, J. L. and Glasgow, E. (2006). The zebrafish bHLH PAS transcriptional regulator, single-minded 1 (sim1), is required for isotocin cell development. *Dev. Dyn.* **235**, 2071-2082.
Eaton, J. L. and Glasgow, E. (2007). Zebrafish orthopedia (otp) is required for isotocin cell development. *Dev. Genes Evol.* **217**, 149-158.
Evans, T. A. and Bashaw, G. J. (2010a). Axon guidance at the midline: of mice and flies. *Curr. Opin. Neurobiol.* **20**, 79-85.
Evans, T. A. and Bashaw, G. J. (2010b). Functional diversity of Robo receptor immunoglobulin domains promotes distinct axon guidance decisions. *Curr. Biol.* **20**, 567-572.
Faraco, J. H., Appelbaum, L., Marin, W., Gaus, S. E., Mourrain, P. and Mignot, E. (2006). Regulation of hypocretin (orexin) expression in embryonic zebrafish. *J. Biol. Chem.* **281**, 29753-29761.
Farmer, W. T., Altick, A. L., Nural, H. F., Dugan, J. P., Kidd, T., Charron, F. and Mastick, G. S. (2008). Pioneer longitudinal axons navigate using floor plate and Slit/Robo signals. *Development* **135**, 3643-3653.
Filippi, A., Dürr, K., Ryu, S., Willaredt, M., Holzschuh, J. and Driever, W. (2007). Expression and function of nr4a2, lmx1b, and pitx3 in zebrafish dopaminergic and noradrenergic neuronal development. *BMC Dev. Biol.* **7**, 135.
Freer, S. M., Lau, D. C., Pearson, J. C., Talsky, K. B. and Crews, S. T. (2011). Molecular and functional analysis of Drosophila single-minded larval central brain expression. *Gene Expr. Patterns* **11**, 533-546.
Fricke, C., Lee, J. S., Geiger-Rudolph, S., Bonhoeffer, F. and Chien, C. B. (2001). astray, a zebrafish roundabout homolog required for retinal axon guidance. *Science* **292**, 507-510.
Fujimoto, E., Stevenson, T. J., Chien, C. B. and Bonkowsky, J. L. (2011). Identification of a dopaminergic enhancer indicates complexity in vertebrate dopamine neuron phenotype specification. *Dev. Biol.* **352**, 393-404.
Furley, A. J., Morton, S. B., Manalo, D., Karagogeos, D., Dodd, J. and Jessell, T. M. (1990). The axonal glycoprotein TAG-1 is an immunoglobulin superfamily member with neurite outgrowth-promoting activity. *Cell* **61**, 157-170.
Golling, G., Amsterdam, A., Sun, Z., Antonelli, M., Maldonado, E., Chen, W., Burgess, S., Haldi, M., Artzt, K., Farrington, S. et al. (2002). Insertional mutagenesis in zebrafish rapidly identifies genes essential for early vertebrate development. *Nat. Genet.* **31**, 135-140.
Hancock, M. B. (1976). Cells of origin of hypothalamo-spinal projections in the rat. *Neurosci. Lett.* **3**, 179-184.
Hohenester, E. (2008). Structural insight into Slit-Robo signalling. *Biochem. Soc. Trans.* **36**, 251-256.
Holst, J., Vignali, K. M., Burton, A. R. and Vignali, D. A. (2006). Rapid analysis of T-cell selection *in vivo* using T cell-receptor retrogenic mice. *Nat. Methods* **3**, 191-197.
Holzschuh, J., Barrallo-Gimeno, A., Ettl, A. K., Durr, K., Knapik, E. W. and Driever, W. (2003). Noradrenergic neurons in the zebrafish hindbrain are induced by retinoic acid and require tfap2a for expression of the neurotransmitter phenotype. *Development* **130**, 5741-5754.
Hutson, L. D., Jurynec, M. J., Yeo, S. Y., Okamoto, H. and Chien, C. B. (2003). Two divergent slit1 genes in zebrafish. *Dev. Dyn.* **228**, 358-369.
Kastenhuber, E., Kern, U., Bonkowsky, J. L., Chien, C. B., Driever, W. and Schweitzer, J. (2009). Netrin-DCC, Robo-Slit, and heparan sulfate proteoglycans coordinate lateral positioning of longitudinal dopaminergic diencephalospinal axons. *J. Neurosci.* **29**, 8914-8926.
Keino-Masu, K., Masu, M., Hinck, L., Leonardo, E. D., Chan, S. S., Culotti, J. G. and Tessier-Lavigne, M. (1996). Deleted in Colorectal Cancer (DCC) encodes a netrin receptor. *Cell* **87**, 175-185.
Kwan, K. M., Fujimoto, E., Grabher, C., Mangum, B. D., Hardy, M. E., Campbell, D. S., Parant, J. M., Yost, H. J., Kanki, J. P. and Chien, C. B. (2007). The Tol2kit: a multisite gateway-based construction kit for Tol2 transposon transgenesis constructs. *Dev. Dyn.* **236**, 3088-3099.
Liu, C., Goshu, E., Wells, A. and Fan, C. M. (2003). Identification of the downstream targets of SIM1 and ARNT2, a pair of transcription factors essential for neuroendocrine cell differentiation. *J. Biol. Chem.* **278**, 44857-44867.
Löhr, H., Ryu, S. and Driever, W. (2009). Zebrafish diencephalic A11-related dopaminergic neurons share a conserved transcriptional network with neuroendocrine cell lineages. *Development* **136**, 1007-1017.
Marion, J. F., Yang, C., Caqueret, A., Boucher, F. and Michaud, J. L. (2005). Sim1 and Sim2 are required for the correct targeting of mammillary body axons. *Development* **132**, 5527-5537.
Michaud, J. L., Rosenquist, T., May, N. R. and Fan, C. M. (1998). Development of neuroendocrine lineages requires the bHLH-PAS transcription factor SIM1. *Genes Dev.* **12**, 3264-3275.
Michaud, J. L., DeRossi, C., May, N. R., Holdener, B. C. and Fan, C. M. (2000). ARNT2 acts as the dimerization partner of SIM1 for the development of the hypothalamus. *Mech. Dev.* **90**, 253-261.
Polleux, F., Ince-Dunn, G. and Ghosh, A. (2007). Transcriptional regulation of vertebrate axon guidance and synapse formation. *Nat. Rev. Neurosci.* **8**, 331-340.
Rink, E. and Wullimann, M. F. (2002). Development of the catecholaminergic system in the early zebrafish brain: an immunohistochemical study. *Brain Res. Dev. Brain Res.* **137**, 89-100.
Ryu, S., Mahler, J., Acampora, D., Holzschuh, J., Erhardt, S., Omodei, D., Simeone, A. and Driever, W. (2007). Orthopedia homeodomain protein is essential for diencephalic dopaminergic neuron development. *Curr. Biol.* **17**, 873-880.
Sabatier, C., Plump, A. S., Ma, L., Brose, K., Tamada, A., Murakami, F., Lee, E. Y. and Tessier-Lavigne, M. (2004). The divergent Robo family protein rig-1/Robo3 is a negative regulator of slit responsiveness required for midline crossing by commissural axons. *Cell* **117**, 157-169.
Spitzweck, B., Brankatschk, M. and Dickson, B. J. (2010). Distinct protein domains and expression patterns confer divergent axon guidance functions for Drosophila Robo receptors. *Cell* **140**, 409-420.
Suli, A., Mortimer, N., Shepherd, I. and Chien, C. B. (2006). Netrin/DCC signaling controls contralateral dendrites of octavolateralis efferent neurons. *J. Neurosci.* **26**, 13328-13337.
Swanson, L. W. (1977). Immunohistochemical evidence for a neurophysin-containing autonomic pathway arising in the paraventricular nucleus of the hypothalamus. *Brain Res.* **128**, 346-353.
Tay, T. L., Ronneberger, O., Ryu, S., Nitschke, R. and Driever, W. (2011). Comprehensive catecholaminergic projectome analysis reveals single-neuron integration of zebrafish ascending and descending dopaminergic systems. *Nat. Commun.* **25**, 171.
Tomasini, A. J., Schuler, A. D., Zebala, J. A. and Mayer, A. N. (2009). PhotoMorphs: a novel light-activated reagent for controlling gene expression in zebrafish. *Genesis* **47**, 736-743.
van den Pol, A. N. (1999). Hypothalamic hypocretin (orexin): robust innervation of the spinal cord. *J. Neurosci.* **19**, 3171-3182.
Wang, W. and Lufkin, T. (2000). The murine Otp homeobox gene plays an essential role in the specification of neuronal cell lineages in the developing hypothalamus. *Dev. Biol.* **227**, 432-449.
Westerfield, M. (1995). *The Zebrafish Book: A Guide for the Laboratory Use of Zebrafish (Danio rerio)*, 3rd edn. Eugene, OR: University of Oregon Press.
Yeo, S. Y., Little, M. H., Yamada, T., Miyashita, T., Halloran, M. C., Kuwada, J. Y., Huh, T. L. and Okamoto, H. (2001). Overexpression of a slit homologue impairs convergent extension of the mesoderm and causes cyclopia in embryonic zebrafish. *Dev. Biol.* **230**, 1-17.
Ypsilanti, A. R., Zagar, Y. and Chédotal, A. (2010). Moving away from the midline: new developments for Slit and Robo. *Development* **137**, 1939-1952.

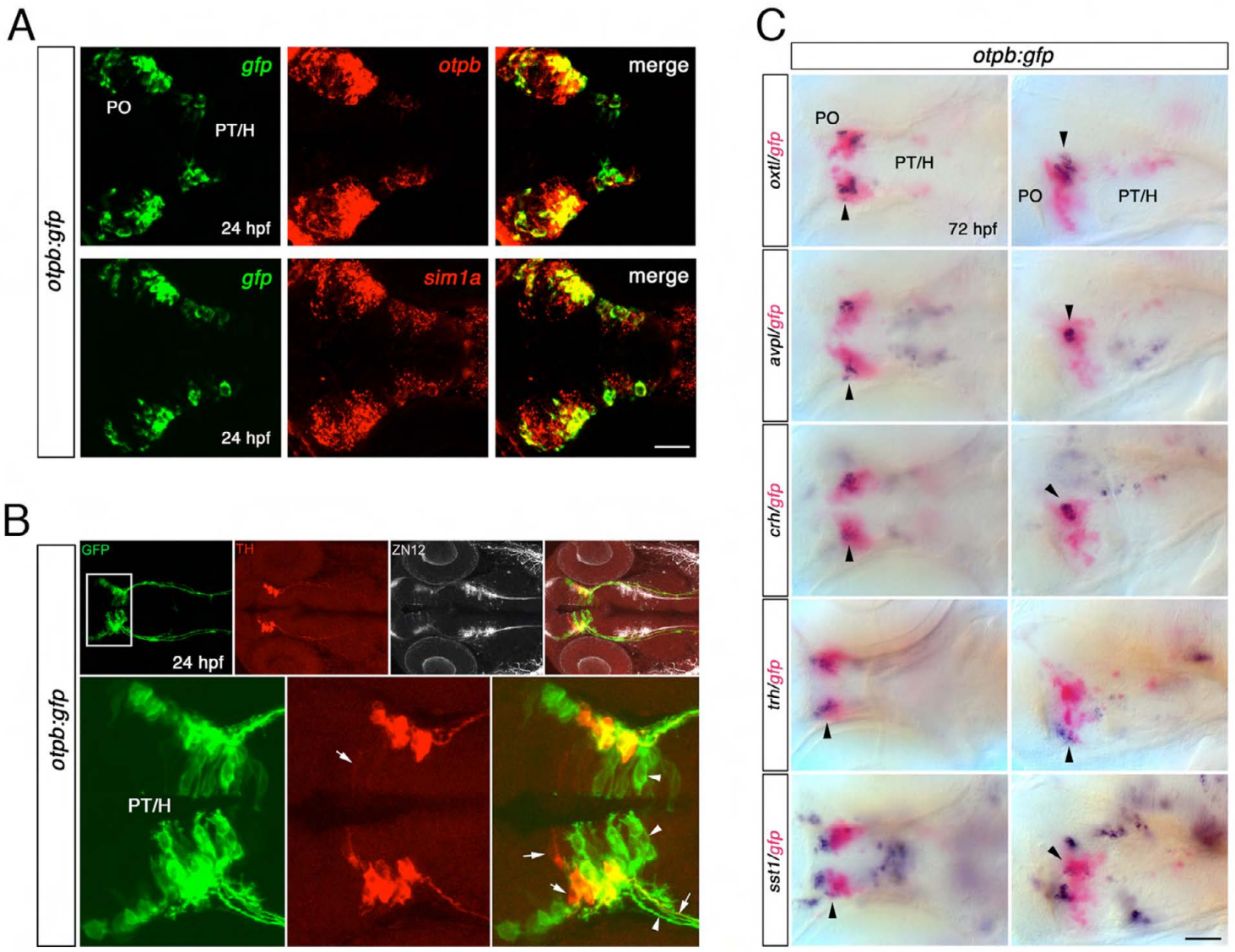

Fig. S1. The *otpb:gfp* reporter line recapitulates many aspects of endogenous *otpb* expression in the forebrain. (**A**) Dorsal views of confocal *z* projections of the forebrain region of *otpb:gfp* transgenic embryos at 24 hpf, demonstrating co-expression of *gfp* (green) and *otpb* (red), as well as co-expression of *gfp* (green) and *sim1a* (red) analyzed by double fluorescent in situ hybridization are shown. Scale bar: 50 μm. (**B**) Dorsal views of *otpb:gfp* transgenic embryos at 24 hpf co-labeled with anti-GFP (green), anti-TH (red) and anti-ZN12. Dopaminergic TH-positive cell bodies and longitudinal dopaminergic projections are immunoreactive for GFP (arrows). Scale bar: 100 μm. (**C**) Dorsal (left panel) and lateral views (right panel) of *otpb:gfp* transgenic embryos at 72 hpf analyzed for co-expression of hypothalamic neurohormones (shown in blue) and *gfp* (shown in purple) by double in situ hybridization. Oxytocin-like (*oxtl*), arginine vasopressin-like (*avpl*), corticotropin releasing hormone (*crh*), thyrotropin releasing hormone (*trh*) and somatostatin 1 (*sst1*) transcripts in the preoptic region all colocalize with *gfp* expression (see arrowheads). Scale bar: 50 μm. PT, posterior tuberculum; H, hypothalamus; PO, preoptic region.

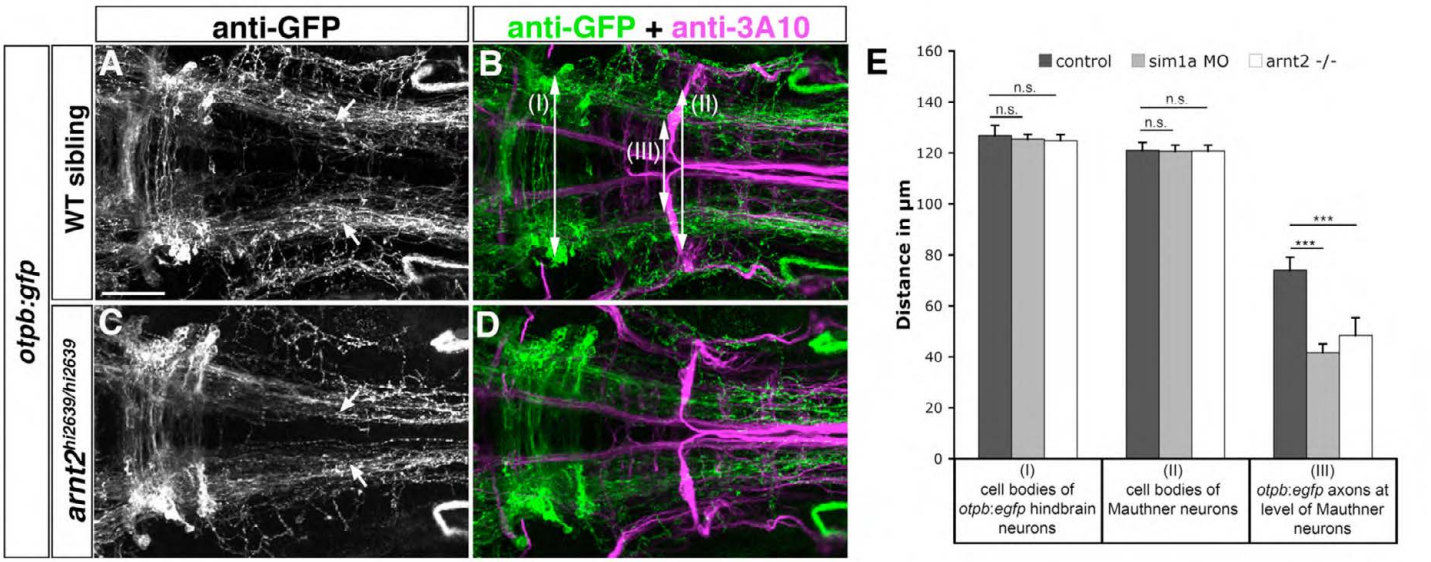

Fig. S2. Lateral positioning of longitudinal *otpb:gfp*-positive axons is altered in *arnt2*^{hi2639c} mutants. Dorsal views of confocal *z* projections of the hindbrain of *otpb:gfp* transgenic embryos co-labeled with anti-GFP and anti-3A10 (A-D) at 72 hpf are shown. (**A**,**B**) Wild-type siblings display normal medio-lateral positioning of *otpb:gfp* positive axons (arrows in A). (**C**,**D**) In *arnt2*$^{hi2639c/hi2639c}$ homozygous mutants, longitudinal projections of *otpb:gfp* axons are shifted towards the midline (arrows in C). Midline crossing of Mauthner axons is not affected in *arnt2*^{hi2639c} mutants, suggesting grossly normal hindbrain development (compare arrowheads in B,D). (**E**) Quantification of mediolateral positioning of *otpb:gfp*-positive longitudinal axons at the anterior-posterior level of Mauthner neurons (see III in B), of the distance of MA neurons (see II in B) and of *otpb:gfp* hindbrain neurons (see I in B) in *arnt2*$^{hi2639c/hi2639c}$ homozygous mutants or wild-type siblings. Numbers in parentheses indicate the number of embryos analyzed. ***P<0.0001; n.s., not significant. Scale bar: 50 µm.

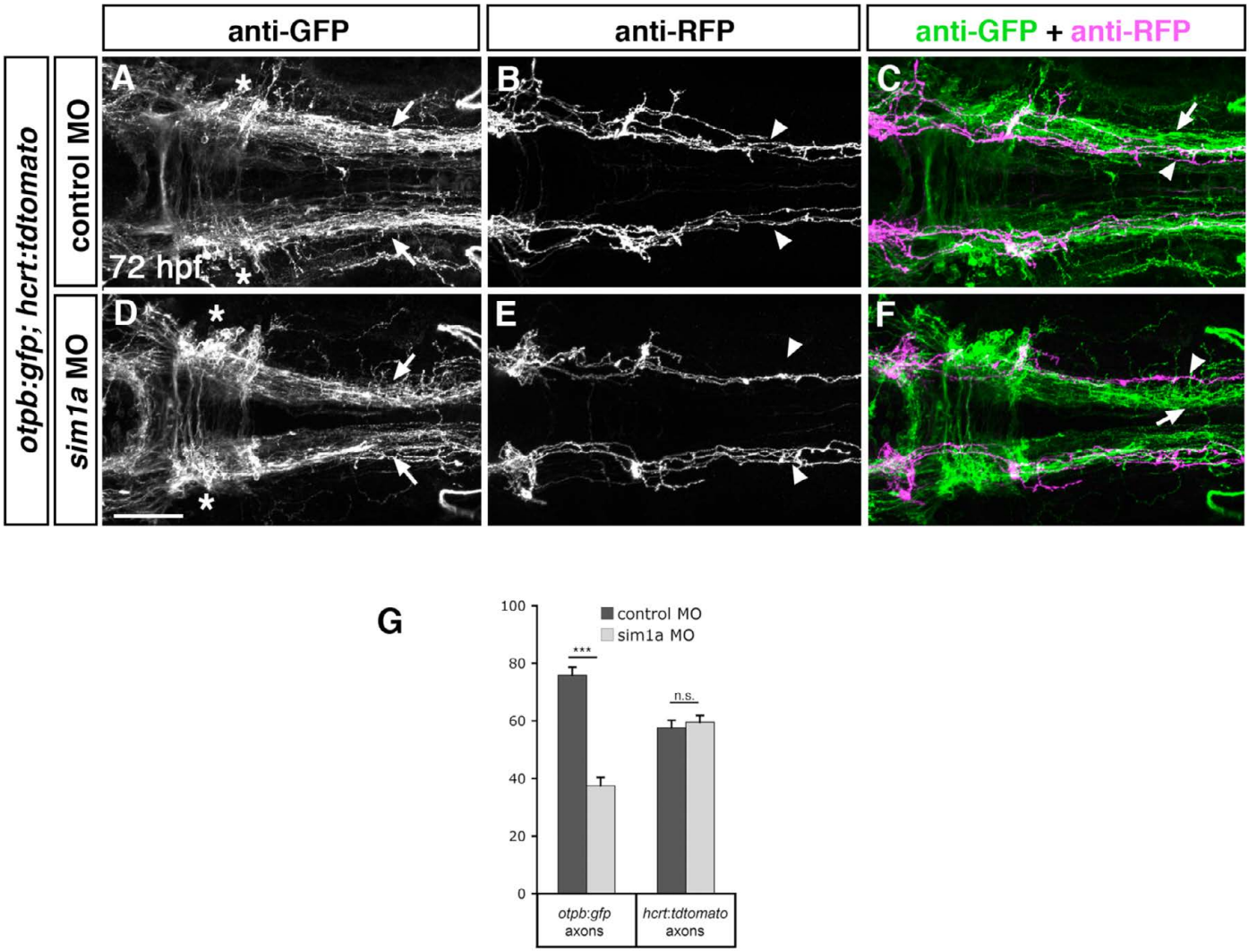

Fig. S3. Loss of Sim1a function causes medial displacement of longitudinal *otpb:gfp*-positive axons. Dorsal views of hindbrain confocal *z* projections of *otpb:gfp;hcrt:tdtomato* double transgenic embryos at 72 hpf. (**A-F**) *otpb:gfp* axons (arrows in D,F) in *sim1a* morphants display strong medial displacement compared with controls (A,C) *hcrt:tdtomato* axons (arrowheads in B,C,E,F) are not affected. *otpb:gfp* hindbrain neurons (asterisks in A,D) do not contribute to longitudinal projections. (**G**) Quantification of mediolateral positioning of *otpb:gfp* and *hcrt:tdtomato* axons at the level of Mauthner neurons at 72 hpf after control or *sim1a* MO injection. ***$P<0.0001$; n.s., not significant. Scale bar: 50 μm for A-F.

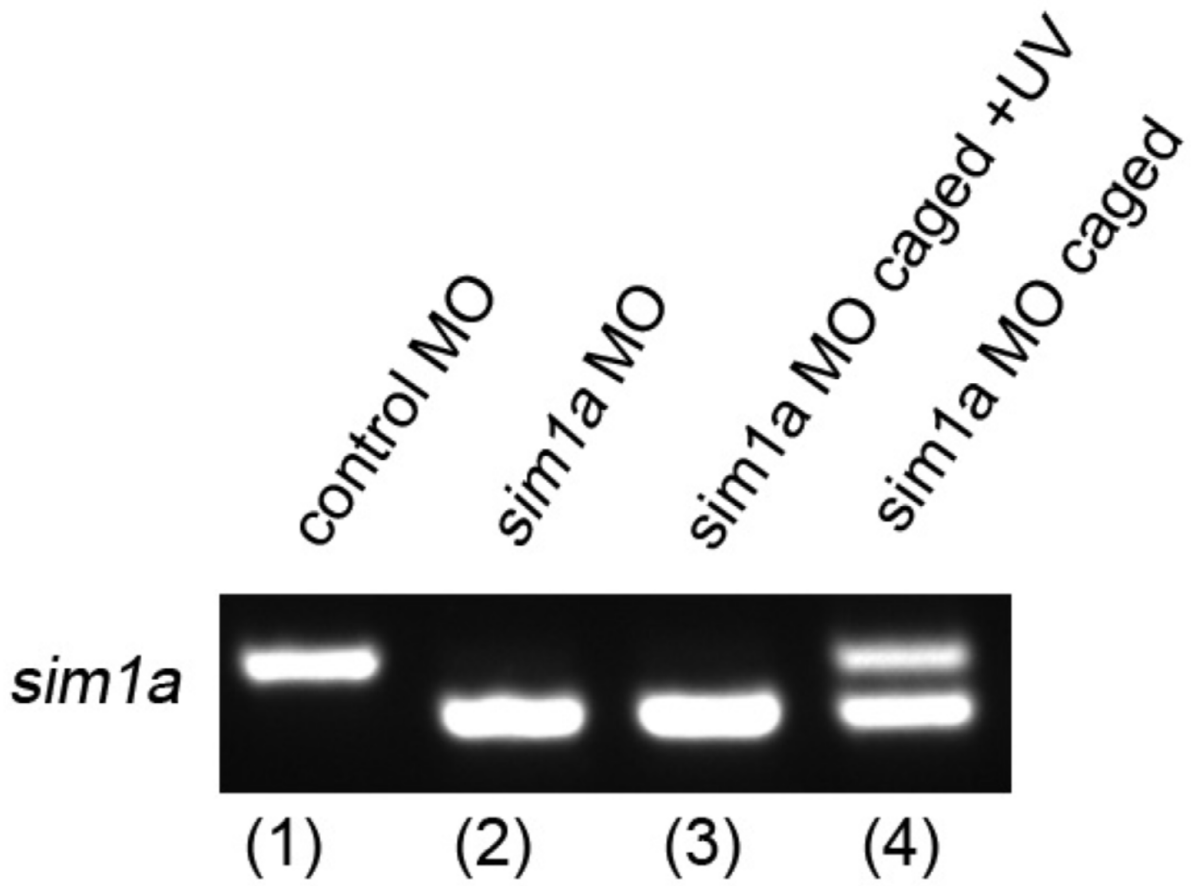

Fig. S4. Temporal control of *sim1a* knockdown using photomorph technology. RT-PCR demonstrating efficacy of temporal control of *sim1a* knockdown. Lane 1, 4.5 ng standard control MO; lane 2, 1 ng *sim1a* MO; lane 3, 1 ng caged *sim1a* MO (=photomorph), which was photocleaved by UV light; lane 4, 1 ng caged *sim1a* MO without UV cleavage. The upper band represents wild-type *sim1a* transcript, the lower band represents the morphant transcript eliminating exon 2. The caging strand never fully blocked the morpholino but instead caused a partial *sim1a* knockdown with residual wild-type transcript. Pooled cDNAs from five injected embryos of each condition were used for analysis.

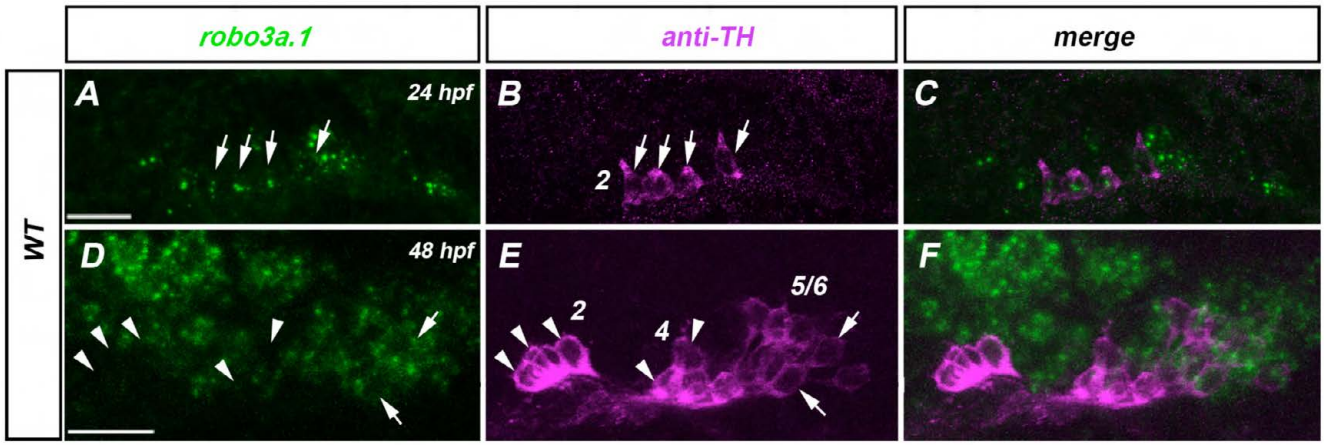

Fig. S5. Expression of *robo3a.1* during development of hypothalamic DA neurons. Dorsal views of confocal *z* projections at the anterior-posterior level of the hypothalamus at indicated developmental stages. Anterior is towards the left. Only the left side of the brain is depicted. (**A-C**) At 24 hpf, expression of *robo3a.1* is found in group 2 TH-positive DA neurons (see arrows in A,B). (**D-F**) At 48 hpf, expression of *robo3a.1* in group 2 and group 4 TH-positive DA neurons is almost undetectable (arrowheads in D-E), whereas group 5-6 TH-positive DA neurons express *robo3a.1*. Numbers in B and E indicate DA neuronal groups according to Rink and Wullimann (Rink and Wullimann, 2002). Scale bars: 25 μm.

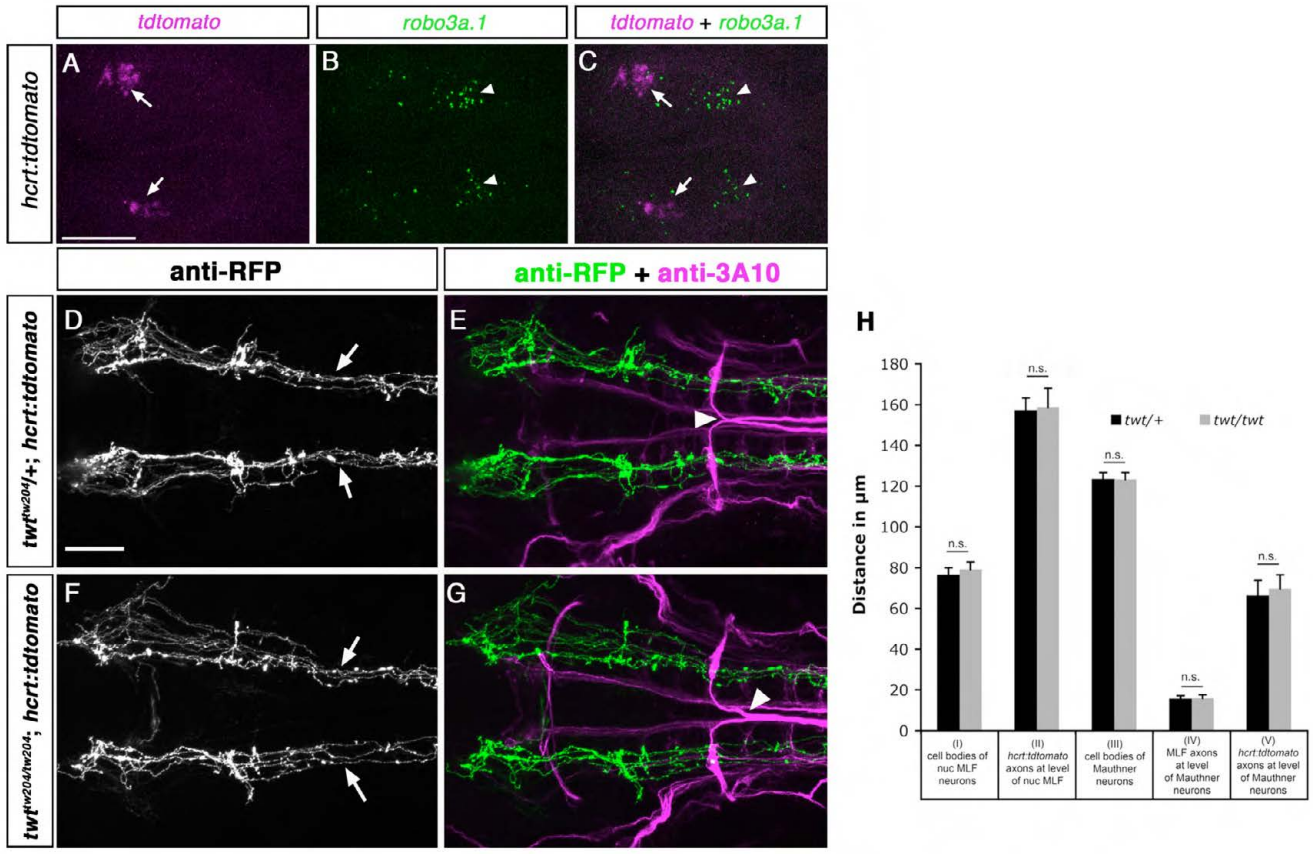

Fig. S6. *robo3* is not required for HTS longitudinal tract formation of Hcrt neurons. Dorsal views of confocal *z* projections of the brain of 24 hpf embryos (A-C) or hindbrain of 72 hpf embryos are shown. Anterior is towards the left. (**A-C**) Whole-mount fluorescent *in situ* hybridization for *tdtomato* and *robo3a.1* expression in *hcrt:tdtomato* embryos are shown. *robo3a.1* (arrowheads in B,C) was not detectable in Hcrt neurons (arrows in A,C). (**D-G**) Immunohistochemistry with anti-RFP and anti-3A10 antibodies demonstrates that pathfinding of TdTomato-positive longitudinal axons is similar in *twt*^{tw204}/+;*hcrt:tdtomato* (arrows in D) when compared with *twt*$^{tw204/tw204}$;*hcrt:tdtomato* embryos (arrows in F). Arrowheads in E indicate normal midline crossing of Mauthner axons in heterozygous *robo3* embryos; arrowhead in G denotes abnormal crossing of Mauthner axons in homozygous *robo3* mutants. (**H**) Quantification of the distance between nucMLF neurons (I) and MLF axons (III), *hcrt:tdtomato* longitudinal axons at two different positions (II +IV) and MA neurons (V) in *twt*/+ and *twt*/*twt* embryos. n.s., not significant. Scale bars: in A, 50 μm for A-C; in D, 50 μm for D-G.

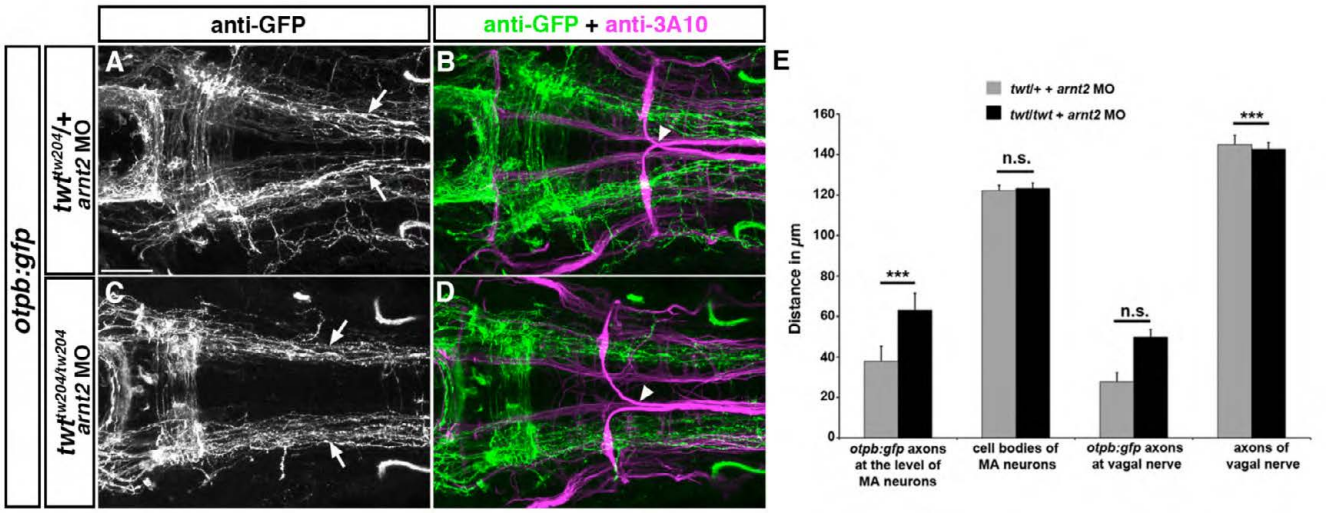

Fig. S7. Medial displacement of *otpb:gfp*-positive longitudinal axons is reduced in *robo3* mutants after *arnt2* knockdown. Dorsal views of *z* projections of the hindbrain of 72 hpf embryos labeled with anti-GFP and anti-3A10 antibodies are shown. Anterior is towards the left. (**A**,**B**) In twt^{tw204}/+;*otpb:gfp* embryos injected with *arnt2* MO *otpb:gfp*-positive longitudinal axons (arrows in A) grow towards the midline. Midline crossing of Mauthner axons is normal (arrowhead in B). (**C**,**D**) After knock down of *arnt2* in $twt^{tw204/tw204}$;*otpb:gfp* embryos, longitudinal axons project in a wild-type manner (arrows in C). Abnormal crossing of Mauthner axons (arrowhead in D) indicates homozygous *robo3* mutant. (**E**) Quantification of the distance of MA neurons and of medio-lateral positioning of *otpb:gfp*-positive longitudinal axons at the anterior-posterior level of Mauthner neurons and medio-lateral positioning of *otpb:gfp* vagal axons. **P*<0.001, Student's *t*-test; n.s., not significant). Scale bar: 50 µm.

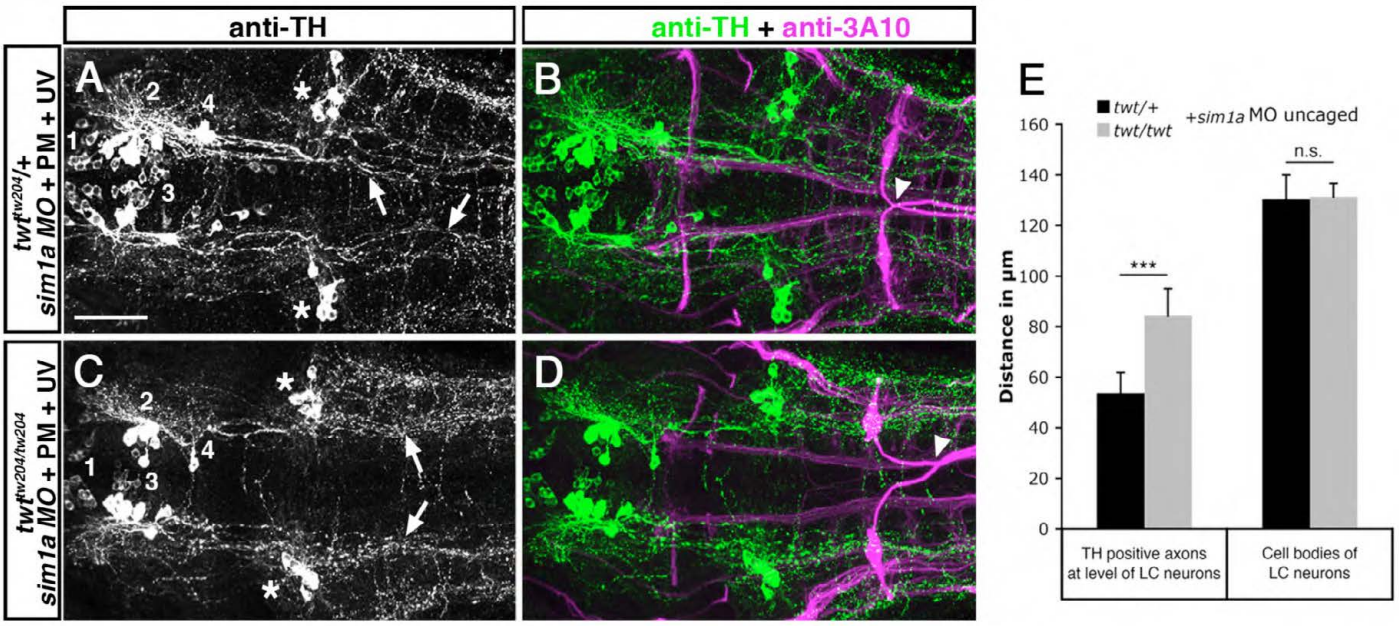

Fig. S8. Medial displacement of TH-positive longitudinal axons in *robo3* mutants is reduced after temporally controlled *sim1a* knockdown. Dorsal views of confocal *z* projections of the hindbrain of 72 hpf embryos labeled with anti-TH and anti-3A10 antibodies are shown. (**A**,**B**) Longitudinal TH-positive axons derived from group 2 and 4 DA neurons are shifted towards the midline (arrows in A) after photoactivation of *sim1a* MO at 22 hpf in twt^{tw204}/+ embryos. Midline crossing of Mauthner axons is normal (arrowhead in B). (**C**,**D**) After temporally controlled activation of *sim1a* MO in $twt^{tw204/tw204}$ embryos at 22 hpf, TH-positive longitudinal axons derived from group 2 and 4 DA neurons project in a wild-type-like fashion (arrows in C). Abnormal crossing of Mauthner axons (arrowhead in D) indicates homozygous *robo3* mutant. (**E**) Quantification of medio-lateral positioning of TH-positive longitudinal axons in $twt^{tw204/+}$ and $twt^{tw204/tw204}$ embryos after temporally controlled activation of *sim1a* MO. Asterisks in A and C indicate noradrenergic locus coeruleus neurons. PM, photomorph; UV, ultra violet. Numbers in A and C indicate DA neuronal groups according to nomenclature of Rink and Wullimann (Rink and Wullimann, 2002). **P*< 0.001, Student's *t*-test; n.s., not significant. Scale bar: 50 µm for A-D.

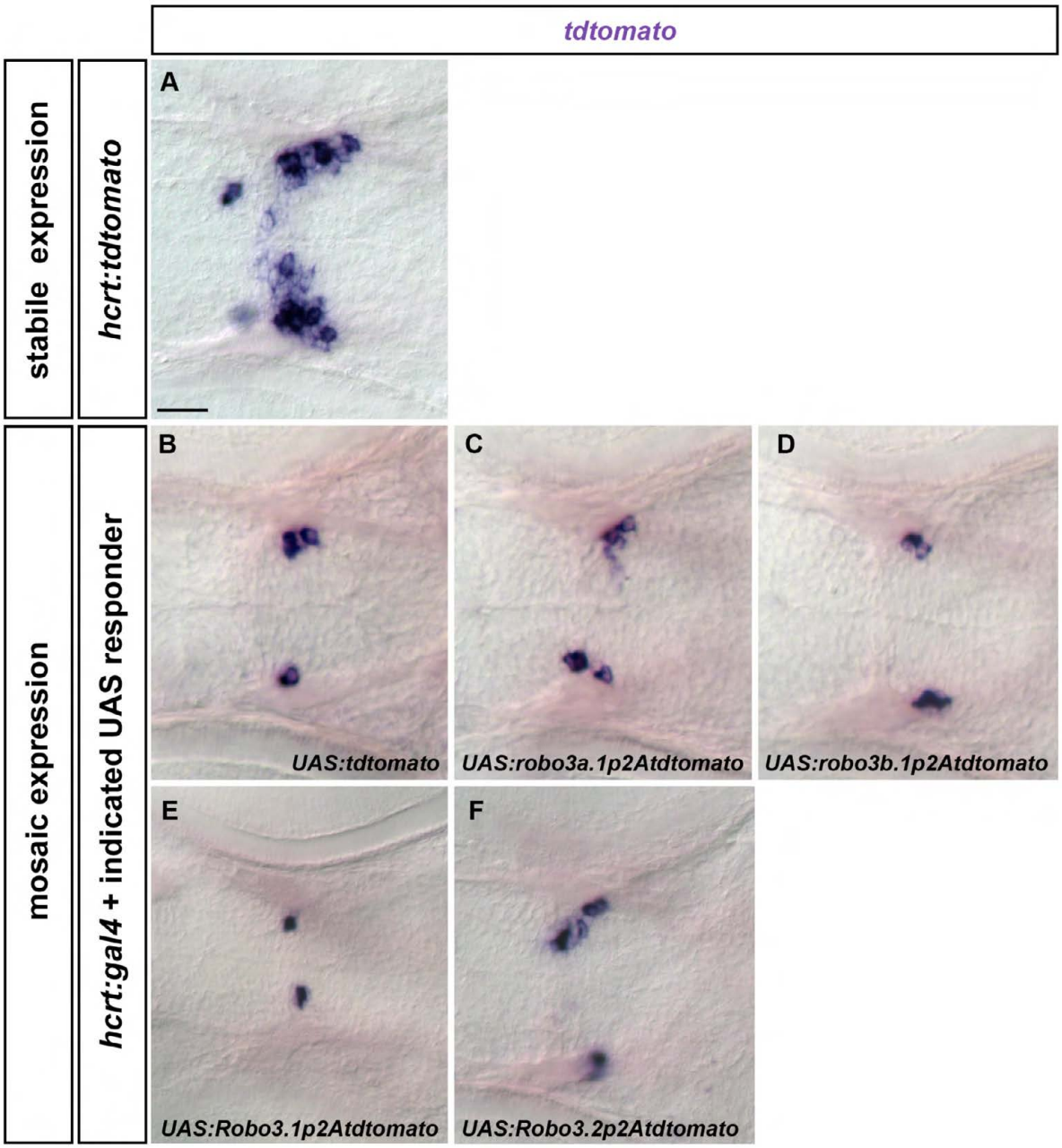

Fig. S9. Expression of *tdtomato* derived from different UAS constructs co-injected with *hcrt:gal4.* Whole-mount *in situ* hybridization showing *tdtomato* expression. Dorsal views of the brain of 72 hpf embryos are shown. Anterior is leftwards. (**A**) Expression of *tdtomato* in a stabile *hcrt:tdtomato* transgenic embryo is shown to illustrate localization of *hcrt* neurons. (**B-F**) Similar levels of transient *tdtomato* expression can be detected after combined injection of *hcrt:gal4* and the indicated UAS constructs. Developing time of the *in situ* hybridization signal for embryos shown in B-D or in E,F was equal. Scale bar: 25 μm.

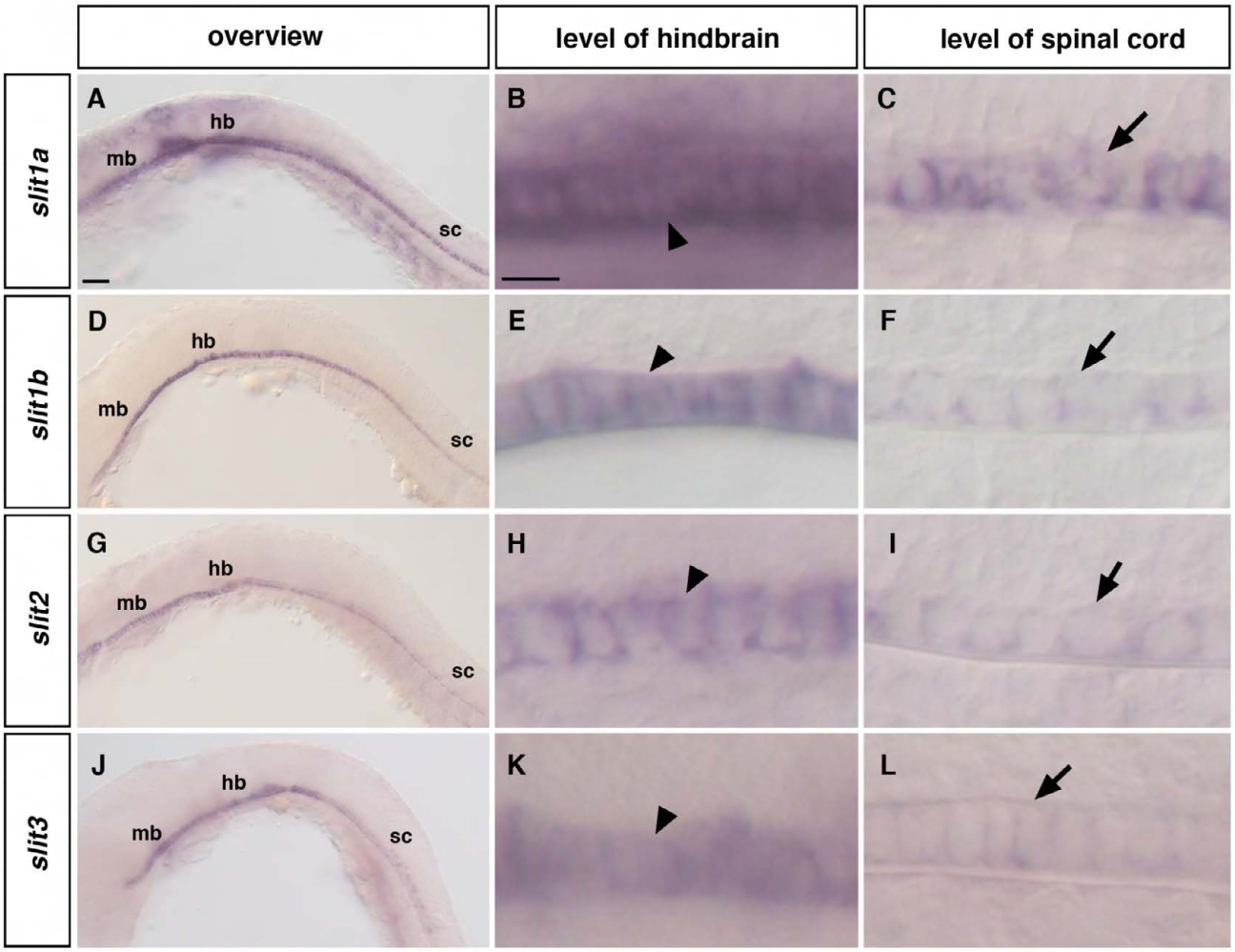

Fig. S10. *slit1*, *slit1b*, *slit2* and *slit3 in situ* hybridization at 24 hpf. Whole-mount in situ hybridization showing *slit1a* (A-C), *slit1b* (D,E), *slit2* (G-I) and *slit3* (J-L) expression. Lateral views of 24 hpf embryos (A,D,G,J), of the floor plate at the level of the hindbrain (B,E,H,K), and of the floor plate at the level of the spinal cord (C,F,I,L) are shown. Anterior to left. (**A-L**) Strong expression of the four different *slit* genes was found in midbrain and hindbrain regions when compared with spinal cord. Higher magnification revealed strong expression of the different slit genes within the floor plate at the level of the hindbrain (arrowheads in B,E,H,K) when compared with floor-plate cells at the level of the spinal cord (arrows in C,F,I,L) mb, midbrain; hb, hindbrain; sc, spinal cord. hb and sc labels also indicate the position of the floor-plate regions shown in higher magnification. Scale bars: in A, 100 μm for A,D,G,J; in B, 50 μm for B,C,E,F,H,I,K,L.

Table S1. Zebrafish mutant/transgenic lines used in this study

Genotype	Reference
arnt2^{hi2639}	Golling et al., 2002
astray (ast^{ti272z}*)*	Fricke et al., 2001
astray (ast^{te284}*)*	Fricke et al., 2001
twitch twice (twt^{tw204}*)*	Burgess et al., 2009
hcrt:tdtomato^{m1163}	This study
hsp70l:robo3b.1iresegfp^{m1217} a.k.a. *hsp70l:robo3b.1*	This study
hsp70l:robo3a.1iresegfp^{m1218} a.k.a *hsp70l:robo3a.1*	This study
Tg*(otpb:1EGFP)*^{zc49} a.k.a *otpb:egfp*	Fujimoto et al., 2011

Table S2. Antibodies and probes

Primary and secondary antibodies for immunohistochemistry	
Anti-Tyrosine Hydroxylase (1:500)	Ryu et al., 2007
Anti-3A10 (1:50)	Furley et al., 1990, Developmental Studies Hybridoma Bank, University of Iowa
Anti-GFP (1:400)	Molecular Probes
Anti-GFP (1:500)	(clone JL-8, Clontech)
Anti-RFP/DsRed/TdTomato (1:500)	MBL
Secondary antibodies were coupled to Alexa-488, Alexa-555 or Alexa-633 (Invitrogen), all used 1:1000.	
List of probes for *in situ* hybridization	
Digoxigenin (Roche), Fluorescein (Roche) or DNP (Molecular Probes) labelled probes were prepared for the following genes: *robo2*, *robo3b.1*, *robo3a.1*, *otpb*, *sim1a*, *oxtl*, *avpl*, *crh*, *trh*, *sst1, slit1a, slit1b, slit2, slit3* and *dcc* (for references see: www.zfin.org). For *gfp* and *tdtomato* probes, partial *gfp* or *tdtomato* coding sequence was subcloned into pCRII-TOPO vector (Invitrogen).	

Table S3. Entry vectors used for multisite gateway system and of complete expression vectors

Vectors	Cloning
p5E-hypocretin	A fragment containing 1 kb hypocretin promoter (Faraco et al., 2006) was subcloned into p5E-MCS.
pME-*robo3b.1* and pME-*robo3a.1*	Full length coding sequences of *robo3* variant 1 (*robo3b.1*) and variant 2 (*robo3a.1*) were amplified from adult brain cDNA and subcloned into pCRII-TOPO (Invitrogen). (robo3b.1_f: 5'- ATGGAGTTTCGCAGGACTTT -3'; robo3a.1_f 5'-ATGCTGCGTTACCTGATAAAGAC-3'; robo3_common_r 5'-TTATCTCATCTCATCATTTCTCTTCCT -3'). Gateway compatible attB1 and attB2 sites were added by PCR. Derived PCR products were recombined into pDONR221 to yield *pME-robo3a.1* and *pME-robo3b.1*.
pME-*Robo3A.1 and* pME-*Robo3A.2*	The mouse *Robo3A.1* and *Robo3A.2* coding sequences were amplified from pCAGGS-*Robo3A.1-myc* or pCAGGS-*Robo3A.2-myc* (Chen et al., 2008) using Gateway-compatible primers. The PCR fragments were subsequently recombined into pDONR221 vector to yield pME-*robo3b.1*, pME-*robo3a.1*, *pME-Robo3A.1* and *pME-Robo3A.2*
pME-tdTomatoCAAX	attB1/B2 sites and a membrane tag encoding the CAAX box of human Harvey Ras (5'-AAGCTGAACCCTCCTGATGAGAGTGGCCCCGGCTGCATGAGCTGCAAGTGTGTGCT CTCCTGA-3') were attached to full length tandemTomato coding sequence (ptdTomatoN1, Clontech) via PCR using Gateway-compatible primers. Derived PCR product was recombined into pDONR221 to yield pME-tdTomatoCAAX.
p3E-P2A-tdTomatoCAAX	att B2r/B3 sites as well as viral P2A (Holst et al., 2006) and human Harvey Ras CAAX cassettes were attached to full length tandemTomato coding sequence via PCR amplification using Gateway-compatible primers and recombined into pDONRP2R-P3 to yield *p3E-P2A-tdTomatoCAAX.*

Subsequent multisite gateway recombination (LR reactions) yielded the desired expression constructs listed below

Cloned expression constructs for transient analyses or generation of stable lines
pDestTol2pA2;hcrt:tdTomatoCAAX-pA
pDestTol2CG2;hcrt:Gal4VP16-pA
pDestTol2CG2;hsp70l:robo3a.1-IRES-EGFP
pDestTol2CG2;hsp70l:robo3b.1-IRES-EGFP
pDestTol2CG2;UAS:robo3a.1-P2A-tdTomatoCAAX
pDestTol2CG2;UAS:Robo3A.1-P2A-tdTomatoCAAX
pDestTol2CG2;UAS:Robo3A.2-P2A-tdTomatoCAAX
pDestTol2CG2;UAS:robo3b.1-P2A-tdTomatoCAAX
pDestTol2CG2;UAS:tdTomatoCAAX-pA

Table S4. Quantification of axon guidance defects after knock down of *sim1a* or *arnt2* (Fig.1 and Fig.S2/S3).

Genotype	***n***	**Injection**	**Average distance between *otpb:gfp longitudinal* axons at the level of the MA neurons**	**Average distance between *hcrt:tdtomato* longitudinal axons at the level of the MA neurons**	**Average distance between MA neurons**
otpb:gfp;hcrt:tdtomato	7	*control* MO (1ng)	75.9 ± 2.7 µm	57.6 ± 2.9 µm	124.2 ± 2.5
otpb:gfp;hcrt:tdtomato	7	*sim1a* MO (1ng)	47.1 ± 5.9 µm	59.5 ± 2.3 µm	122.8 ± 2.6

Genotype	***n***	**Injection**	**Average distance between *otpb:gfp* longitudinal axons at the level of the MA neurons**	**Average distance between MA neurons**
otpb:gfp	14	control MO (4.5 ng)	69.7 ± 7.3 µm	124.1 ± 1.7
otpb:gfp	14	*sim1a* MO (1 ng)	42.6 ± 3.9 µm	123.3 ± 2.6
otpb:gfp	16	*sim1a* MO (0.25 ng)	69.4 ± 3.4 µm	125.2 ± 2.3
arnt2^{hi2639c}, otpb:gfp	9		48.4 ± 6.9 µm	124.2 ± 3.9
otpb:gfp	13	*arnt2* MO (4.5 ng)	44.5 ± 5.6 µm	124.7 ± 2.6 µm
otpb:gfp	15	*arnt2* MO (1 ng)	67.3 ± 2.6 µm	124.3 ± 1.7 µm
otpb:gfp	16	*arnt2* MO (1 ng) + *sim1a* MO (0.25 ng)	42.5 ± 8.2 µm	123.1 ± 2.5 µm

Genotype	***n***	**Injection**	**Average distance between *otpb:gfp* neurons in hindbrain**
otpb:gfp	14	control MO	126.3 ± 3.8 µm
otpb:gfp	14	*sim1a* MO	125.5 ± 1.7 µm
otpb:gfp	16	*sim1a* MO (0.25 ng)	124.8 ± 3.2 µm
arnt2^{hi2639c}, otpb:gfp	9		124.4 ± 2.8 µm
otpb:gfp	13	*arnt2* MO (4.5 ng)	125.6 ± 2.6 µm
otpb:gfp	15	*arnt2* MO (1 ng)	124.4 ± 2.7 µm
otpb:gfp	16	*arnt2* MO (1 ng) + *sim1a* MO (0.25 ng)	124.3 ± 3.4 µm

To quantify the axon guidance phenotypes upon depletion of *sim1a* or *arnt2*, we determined the distance between the *otpb:gfp* or *hcrt:tdtomato* longitudinal axons at the level of the Mauthner neurons (Fig. S2B). To control for the specificity of the observed effects, we measured the distance between the MA neurons and between the *otpb:gfp* neurons in the hindbrain (Fig. S2B). For *otpb:gfp* longitudinal axons. This analysis revealed a significant difference in the distance of longitudinal *otpb:gfp* axons upon injection of 1 ng *sim1a* MO, 4.5 ng *arnt2* MO or in *arnt2^{hi2639c}* mutants when compared with 0.25 ng *sim1a* MO-, 1 ng *arnt2* MO- or 4.5 ng control MO-injected embryos. The amount of injected MO is indicated as ng/embryo. The distance between longitudinal *hcrt:tdtomato* axons, MA neurons or hindbrain *otpb:gfp* neurons was not different.

Table S5. Quantifications of HTS axon guidance defects observed in *sim1a* photomorph experiment (see Fig. 2)

Genotype	***n***	**Injection**	**Average distance between longitudinal TH positive axons at the level of the LC neurons**	**Average distance between LC neurons**
otpb:gfp	13	*sim1a + PM + UV*	54.1 ± 6.9 µm	129.2 ± 2.3 µm
otpb:gfp	12	control MO	83.7 ± 5.4µm	129.1 ± 3.1 µm
Genotype	***n***	**Injection**	**Average distance of group 2 DA neurons toward the midline (left and right side combined**	**Average distance of group 4 DA neurons toward the midline (left and right side combined**
otpb:gfp	13	*sim1a + PM + UV*	32.1 ± 6.9 µm	36.5 ± 5.5 µm
otpb:gfp	12	control MO	33.2 ± 3.4 µm	34.1 ± 3.6 µm
Genotype	***n***	**Injection**	**Average distance between MA neurons**	
otpb:gfp	11	sim1a + PM + UV	123.6 ± 2.3 µm	
otpb:gfp	10	control MO	124.1 ± 2.2 µm	

To quantify the axon guidance effects in *sim1a* photomorph experiments, we measured the distance between longitudinal TH-positive axons at the anterior-posterior level of noradrenergic locus coeruleus (LC) neurons (Fig. 2B). To control for specificity of the observed effects, we determined the distance between the cell bodies of LC neurons (Fig. 2B) and of the MA neurons. In addition, we determined the distance of group 2 and 4 DA neurons from the midline (Fig. 2A). This analysis demonstrated a significant decrease of the distance between TH-positive longitudinal axons in *sim1a* photomorphants when compared with control MO-injected embryos. The distance between the LC neurons or MA neurons or positioning of DA neurons was not altered.

Absolute values with s.d. of average distances in µm are shown; *n* indicates number of embryos analyzed.

Table S6. Quantification of axon guidance defects in *robo2* mutant larvae (Fig. 3)

Genotype	***n***	**Average distance between longitudinal *otpb:gfp* axons at the level of the MA neurons**	**Average distance between longitudinal *hcrt:tdtomato* axons at the level of the MA neurons**	**Average distance between MA neurons**
ast^{ti272z}/+;*otpb:gfp*;*hcrt:tdtomato*	6	41.9± 5.4 µm	39.3± 5.4 µm	122.3± 3.5 µm
ast$^{ti272z/ti272z}$;*otpb:gfp*;*hcrt:tdtomato*	7	15.3± 2.7 µm	18.2± 5.3 µm	121.7± 2.5 µm

For quantification we determined the distance between *otpb:gfp* axons and *hcrt:tdtomato* axons at the level of the Mauthner neurons. To control for specificity, we determined the distance between MA neurons. This analysis demonstrated a significant decrease of the distance between *otpb:gfp* and *hcrt:tdtomato* longitudinal axons in *ast* mutants when compared with heterozygous *ast* controls. Distance between MA neurons was not different.

Absolute values with s.d. of average distances in µm are shown; *n* indicates number of embryos analyzed.

Table S7. Quantification of axon guidance defects in *robo3/twt* mutant larvae (Fig. 5 and Fig. S8)

Genotype	***n***	**Average distance between longitudinal *otpb:gfp* or *hcrt:tdtomato* axons at the level of the nucMLF neurons**	**Average distance between longitudinal *otpb:gfp* or *hcrt:tdtomato* axons at the level of the Mauthner neurons**
twt$^{tw204/+}$;*otpb:gfp*	21	182.9 ± 8.7 µm	64.8 ± 4.7 µm
twt$^{tw204/tw204}$;*otpb:gfp*	21	201.1 ± 10.8 µm	77.4 ± 6.2 µm
twt^{tw204}/+;*hcrt:tdtomato*	16	156.9 ± 9.4 µm	69.7 ± 7.8 µm
twt$^{tw204/tw204}$;*hcrt:tdtomato*	17	158.7 ± 9.4 µm	66.2 ± 7.6 µm

Genotype	***n***	**Average distance between nucMLF neurons in midbrain**	**Average distance between nucMLF axons at the level of MA neurons**
twt$^{tw204/+}$;*otpb:gfp*	21	77.9 ± 2.8 µm	14.6 ± 1.6 µm
twt$^{tw204/tw204}$;*otpb:gfp*	21	78.3 ± 2.4 µm	14.8 ± 1.6 µm
twt^{tw204}/+;*hcrt:tdtomato*	16	76.3 ± 3.6 µm	15.8 ± 1.8 µm
twt$^{tw204/tw204}$;*hcrt:tdtomato*	17	79.1 ± 3.6 µm	15.5 ± 1.6 µm

Genotype	***n***	**Average distance between MA neurons**
twt$^{tw204/+}$;*otpb:gfp*	21	123.2 ± 2.5 µm
twt$^{tw204/tw204}$;*otpb:gfp*	21	123.4 ± 3.8 µm
twt^{tw204}/+;*hcrt:tdtomato*	16	123.3 ± 3.2 µm
twt$^{tw204/tw204}$;*hcrt:tdtomato*	17	123.2± 3.3 µm

To analyze the role of *robo3* during HTS longitudinal axon guidance, the distance between *otpb:gfp* or *hcrt:tdtomato* longitudinal axons was determined at two different positions (see Fig. 5B). The first measurement was taken at the level of nucMLF neurons in the midbrain, shortly posterior to the level where *otpb:gfp*-positive axons have left the diencephalon. The second measurement was taken in the hindbrain at the level of the Mauthner neurons. To control for the specificity of the observed effects, we determined the distance between the nucMLF neurons and the distance between the nucMLF axons at the level of the Mauthner neurons (Fig. 5D,E). In addition, we determined the distance between the MA neurons. This analysis revealed a significant difference in the distance of longitudinal *otpb:gfp* axons in homozygous *twt* mutants when compared with heterozygous *twt* siblings. The distance between longitudinal *hcrt:tdtomato* axons, nucMLF neurons and their axons and the between the MA neurons was not different in either genotype (Fig.5E, Fig. S8H).

Absolute values with s.d. of average distances in µm are shown; *n* indicates number of embryos analyzed.

Table S8. Quantifications of axon tract position defects after *sim1a* or *arnt2* depletion experiments in *robo3/twt* mutant background (Fig. 5 and Fig. S9)

Genotype	***n***	**Injection**	**Average distance between *otpb:gfp* vagal nerve at ventral turning point**	**Average distance between *otpb:gfp* longitudinal axons at ventral turning point of potential vagal nerve**
twt$^{tw204/}$+;*otpb:gfp*	17	*sim1a* MO	141.5 ± 7.5 µm	22.3 ± 3.4 µm
twt$^{tw204/tw204}$;*otpb:gfp*	18	*sim1a* MO	144.5 ± 10.3 µm	47.1 ± 5.9 µm
twt$^{tw204/}$+;*otpb:gfp*	7	*arnt2* MO	142.4 ± 4.5 µm	27.7 ± 3.3 µm
twt$^{tw204/tw204}$;*otpb:gfp*	7	*arnt2* MO	144.8 ± 4.4 µm	49.9 ± 3.7 µm
Genotype	***n***	**Injection**	**Average distance between MA neurons**	**Average distance between *otpb:gfp* longitudinal axons at level of MA neurons**
twt$^{tw204/}$+;*otpb:gfp*	17	*sim1a* MO	122.1 ± 3.2 µm	21.9 ± 6.1
twt$^{tw204/tw204}$;*otpb:gfp*	18	*sim1a* MO	121.6 ± 3.4 µm	44.1 ± 7.6
twt$^{tw204/}$+;*otpb:gfp*	7	*arnt2* MO	122.2 ± 2.7 µm	37.8 ± 7.4
twt$^{tw204/tw204}$;*otpb:gfp*	7	*arnt2* MO	123.3 ± 2.7 µm	63.2 ± 8.2

In order to analyze the effect upon *sim1a* or *arnt2* depletion on longitudinal *otpb:gfp* axons in *twt* mutants, the distance between the bilateral *otpb:gfp*-positive longitudinal axon bundles was determined. To control for specificity, the distance between *otpb:gfp*-positive axons potentially derived from Xth (vagal) nerve neurons was determined. Both measurements were taken at an anterior-posterior level where the *otpb:gfp* positive potential vagal nerve axons turn ventrally (arrows in Fig. 5G). In addition, the distance between the MA neurons was determined. This analysis demonstrated a significant larger distance between *otpb:gfp* longitudinal axons in *twt* homozygous mutants after depletion of *sim1a* or *arnt2* when compared with heterozygous *twt* embryos. The distance between *otpb:gfp* vagal nerves or MA neurons was not different in either genotype (Fig. 5J and Fig. S9E).

Absolute values with s.d. of average distances in µm or average numbers are shown; *n* indicates number of embryos analyzed.

Table S9. Quantification of axon tract position defects after *sim1a* photomorph experiments in *robo3* mutant background (Fig. S10)

Genotype	***n***	**Injection**	**Average distance between LC neurons**	**Average distance between longitudinal TH positive axons at the level of the LC neurons**
twt$^{tw204/}$+	11	*sim1a* MO + PM	130.1 ± 9.8 µm	54,4 ± 8,4 µm
twt$^{tw204/tw204}$	12	*sim1a* MO + PM	131.2 ± 5.2 µm	84,3 ± 10,6 µm
Genotype	***n***	**Injection**	**Average distance between MA neurons**	
twt$^{tw204/+}$	7	*sim1a MO + PM*	121.5 ± 2.8 µm	
twt$^{tw204/tw204}$	7	*sim1a MO + PM*	123.3 ± 1.1 µm	

To analyze the effect upon *sim1a* photomorph experiment in *twt* mutants, we measured the distance between longitudinal TH-positive axons at the anterior-posterior level of noradrenergic LC neurons. Normal hindbrain development was confirmed by comparing the distance between the LC neurons, which was similar in *twt* heterozygous and mutant embryos. This analysis revealed a significant difference in the distance of TH-positive longitudinal axons in *twt* homozygous photomorphants when compared with heterozygous *twt* embryos. The distance of LC neurons or MA neurons was not different in either genotype (Fig. S10E).

Absolute values with s.d. of average distances in µm or average numbers are shown; *n* indicates number of embryos analyzed.

Table S10. Quantification of axon positions after overexpression of *robo3a.1* or *robo3b.1* in *otpb:gfp* background (Fig. 6A-G)

Genotype	*n*	Average number of *otpb:gfp* axons in inner segment	Average distance between MA neurons
otpb:gfp	16	0.9 ± 0.8	104.9 ± 4.1 µm
otpb:gfp; hsp70l:robo3a.1	16	2.9 ± 1.2	102.9 ± 6.5 µm
otpb:gfp, hsp70l:robo3b.1	16	0.7 ± 0.8	106.3 ± 6.0 µm

To quantify the effects after overexpression of *robo3a.1* or *robo3b.1*, we counted the number of longitudinal *otpb:gfp* longitudinal axons in an inner section, as defined by the distance between the MA neurons (Fig. 6B,B′,D,F). To control for specificity, we determined the distance of the MA neurons. This analysis revealed a significant increase in the number of longitudinal *otpb:gfp* axons in the inner section after overexpression of *robo3a.1* when compared with controls or after *robo3b.1* overexpression (Fig. 6A-G). This distance of the MA neurons was not different among the experimental groups.

Absolute values with s.d. of average distances in µm or average numbers are shown; *n* indicates number of embryos analyzed.

Table S11. Quantification of axon positions after overexpression of *robo3a.1* or *robo3b.1* in *hcrt:tdtomato* background (Fig. 6H-N)

Genotype	*n*	Average number of *hcrt:tdtomato* axons in outer segments	Average number of *hcrt:tdtomato* axon in inner segments	Average total number of *hcrt:tdtomato* axons	Average distance between MA neurons
hcrt:tdtomato	18	9.2 ± 1.5	0.6 ± 0.8	9.8 ± 1.5	131.1 ± 7.6 µm
hcrt:tdtomato; hsp70l:robo3a.1	19	6.1 ± 1.3	3.7 ± 0.7	9.8 ± 1.5	127.9 ± 6.9 µm
hcrt:tdtomato, hsp70l:robo3b.1	18	8.5 ± 0.9	0.7 ± 0.8	9.2 ± 1.2	127.2 ± 6.1 µm
Genotype		**Average distance of anterior Hcrt neurons toward the midline (left and right side combined)**			
hcrt:tdtomato	10	30.4 ± 3.1			
hcrt:tdtomato; hsp70l:robo3a.1	10	30.2 ± 2.3			
hcrt:tdtomato, hsp70l:robo3b.1	10	30.1 ± 3.4			

To quantify the effects after overexpression of *robo3a.1* or *robo3b.1*, we divided the hindbrain at the anterior-posterior level of the Mauthner neurons into an inner (medial) and two outer (lateral) sections (Fig. 6I), and counted the number of longitudinal *hcrt:tdtomato* axons in each section. To control for specificity, we determined the distance of the MA neurons and the distance of the most anterior Hcrt neurons. This analysis revealed a significant increase in the number of longitudinal *hcrt:tdtomato* axons in the inner section after overexpression of *robo3a.1* when compared with controls or after *robo3b.1* overexpression (Fig. 6F-H,M). This distance of the MA or Hcrt neurons was not different among the experimental groups.

Absolute values with s.d. of average distances in µm or average numbers are shown; *n* indicates number of embryos analyzed.

Table S12. Quantification axon positions after combined injections of *sim1a* and *dcc* in *otpbgfp* embryos (Fig. 7)

Genotype	*n*	Injection	Average distance between longitudinal *otpb:gfp* axons at the level of the Mauthner neurons	Average distance between Mauthner neurons
otpb:gfp	22	*sim1a* MO and control MO	27.9 ± 4.4 µm	116.9 ± 1.7 µm
otpb:gfp	23	*sim1a* MO and *dcc* MO	50.2 ± 8.1 µm	117.4 ± 1.3 µm

To analyze longitudinal *otpb:gfp* axon guidance after combined knock down of *sim1a* and *dcc*, we measured the average distance between the closest *otpb:gfp*-positive longitudinal axons at the level of the Mauthner neurons. This analysis revealed an increased distance of longitudinal axons upon depletion of *sim1a* and *dcc* when compared with controls. To control for specificity, we determined the distance between the MA neurons, which was not different (Fig. 7B,E).

Absolute values with standard deviations of average distances in µm or average numbers are shown;
n indicates number of embryos analyzed.

Table S13. Quantification of axon positions after injection of *sim1a* or control MO into *ast ;twt* compound mutants (Fig. 8)

Genotype	*n*	Injection	Distance between *otpb:gfp* vagal nerve at ventral turning point	Distance between *otpb:gfp* longitudinal axons at ventral turning point of potential vagal nerve
twt^{tw204}/+;*ast*$^{ti272z/ti272z}$ *otpb:gfp*	16	*sim1a* MO	129.4 ± 2.9 µm	15.2 ± 2.7 µm
twt$^{tw204/tw204}$;*ast*$^{ti272z/ti272z}$;*otpb:gfp*	16	*sim1a* MO	132.1 ± 3.7 µm	15.6 ± 2.3 µm
twt$^{tw204/tw204}$;*ast*$^{ti272z/ti272z}$;*otpb:gfp*	16	Control MO	128.1 ± 3.5 µm	15.6 ± 2.5 µm
Genotype	***n***	**Injection**	**Average distance between Mauthner neurons**	**Distance between *otpb:gfp* longitudinal axons at level of MA neurons**
twt^{tw204}/+;*ast*$^{ti272z/ti272z}$ *otpb:gfp*	16	*sim1a* MO	120.9 ± 2.3 µm	14.4 ± 1.9 µm
twt$^{tw204/tw204}$;*ast*$^{ti272z/ti272z}$;*otpb:gfp*	16	*sim1a* MO	120.8 ± 2.7 µm	16.5 ± 2.1 µm
twt$^{tw204/tw204}$;*ast*$^{ti272z/ti272z}$;*otpb:gfp*	16	Control MO	122.3 ± 2.5 µm	16.1 ± 2.3 µm

To determine medial displacement phenotype in *sim1a* or control MO-injected *ast;twt* compound mutant embryos, we measured the distances between *otpb:gfp* longitudinal axons and vagal axons. In addition, the distance between the MA neurons was determined. This analysis revealed no differences for the measurements.

Absolute values with standard deviations of average distances in µm or average numbers are shown;
n indicates number of embryos analyzed.

Table S14. Quantification of axon positions after overexpression of *robo3a.1* in weak and strong *ast* mutants (Fig. 9)

Genotype	***n***	**Average number of *hcrt:tdtomato* axons in outer segments**	**Average number of *hcrt:tdtomato* axon in inner segments**	**Average total number of *hcrt:tdtomato* axons**	**Average distance between MA neurons**
ast$^{ti272z/ti272z}$; hcrt:tdtomato	18	1.3 ± 1.4	8.7 ± 1.2	9.5 ± 2.6	130.1 ± 6.8 µm
ast$^{ti272z/ti272z}$; hcrt:tdtomato; hsp70l:robo3a.1	18	1.8 ± 1.5	7.2 ± 1.7	9.6 ± 1.6	129.1 ± 6.5 µm
ast$^{te284/te284}$; hcrt:tdtomato	17	4.7 ± 1.7	3.7 ± 1.6	8.4 ± 0.9	126.3 ± 3.8 µm
ast$^{te284/te284}$; hcrt:tdtomato; hsp70l:robo3a.1	17	1.3 ± 0.9	6.7 ± 1.0	8.1 ± 1.1	125.1 ± 4.5 µm
Genotype	***n***	**Average distance of anterior Hcrt neurons toward the midline (left and right side combined)**			
ast$^{ti272z/ti272z}$; hcrt:tdtomato	10	31.3 ± 2.6			
ast$^{ti272z/ti272z}$; hcrt:tdtomato; hsp70l:robo3a.1	10	30.9 ± 2.7			
ast$^{te284/te284}$; hcrt:tdtomato	10	29.9 ± 2.7			
ast$^{te284/te284}$; hcrt:tdtomato; hsp70l:robo3a.1	10	30.5 ± 2.6			

The effects upon overexpression of *robo3a.1* in the weak and strong *ast* mutant background were quantified by making use of the inner and outer sections (Fig. 9B,F,K,O) as described above for Fig. 6. This analysis revealed a significant increase in the number of longitudinal *hcrt:tdtomato* axons in the inner section after overexpression of *robo3a.1* in the weak *ast* mutants when compared with controls or the strong *ast* mutants (Fig. 9I,R). To control for specificity, we determined the distance of the MA neurons or the distance of the most anterior Hcrt neurons, which was not different.
Absolute values with s.d of average distances in µm or average numbers are shown; *n* indicates number of embryos analyzed.

Table S15. Quantification of MA neuron distance after overexpression of *robo3a.1*, *robo3b.1*, *Robo3A.1* and *Robo3A.2* using GAL4/UAS approach (Fig. 10)

Injection	***n***	**Average distance between MA neurons**
UAS:tdtomato	22	123.3 ± 3.5 µm
UAS:robo3a.1p2Atdtomato	23	123.3 ± 2.2 µm
UAS:robo3b.1p2Atdtomato	21	122.5 ± 2.9 µm
UAS:Robo3A.1p2Atdtomato	20	122.6 ± 4.4 µm
UAS:Robo3A.2p2Atdtomato	21	122.3 ± 4.7 µm
Injection	***n***	**Average distance between Hcrt neurons**
UAS:tdtomato	10	29.3 ± 3.3
UAS:robo3a.1p2Atdtomato	10	29.2 ± 3.7
UAS:robo3b.1p2Atdtomato	10	30.2 ± 4.2
UAS:Robo3A.1p2Atdtomato	10	30.4 ± 4.7
UAS:Robo3A.2p2Atdtomato	10	30.1 ± 3.6

To control for specificity upon mis-expression of the different *robo3* isoforms using a *hcrt:gal4* driver in combination with the UAS constructs mentioned below, we determined the distance of the MA and Hcrt neurons, which was not different.
Absolute values s.d. of average distances in µm or average numbers are shown; *n* indicates number of embryos analyzed.